2015

AIRBORNE PATH FREQUENCY BASED SUBSTRUCTURING METHOD AND ITS APPLICATIONS

Rui He
University of Kentucky, herui1989@gmail.com

STUDENT AGREEMENT:

I represent that my thesis or dissertation and abstract are my original work. Proper attribution has been given to all outside sources. I understand that I am solely responsible for obtaining any needed copyright permissions. I have obtained needed written permission statement(s) from the owner(s) of each third-party copyrighted matter to be included in my work, allowing electronic distribution (if such use is not permitted by the fair use doctrine) which will be submitted to UKnowledge as Additional File.

I hereby grant to The University of Kentucky and its agents the irrevocable, non-exclusive, and royalty-free license to archive and make accessible my work in whole or in part in all forms of media, now or hereafter known. I agree that the document mentioned above may be made available immediately for worldwide access unless an embargo applies.

I retain all other ownership rights to the copyright of my work. I also retain the right to use in future works (such as articles or books) all or part of my work. I understand that I am free to register the copyright to my work.

REVIEW, APPROVAL AND ACCEPTANCE

The document mentioned above has been reviewed and accepted by the student's advisor, on behalf of the advisory committee, and by the Director of Graduate Studies (DGS), on behalf of the program; we verify that this is the final, approved version of the student's thesis including all changes required by the advisory committee. The undersigned agree to abide by the statements above.

Rui He, Student

Dr. David W. Herrin, Major Professor

Dr. Haluk E. Karaca, Director of Graduate Studies

AIRBORNE PATH FREQUENCY BASED SUBSTRUCTURING METHOD AND ITS APPLICATIONS

THESIS

A thesis submitted in partial fulfillment of the
requirements for the degree of Master of Science
in Mechanical Engineering in the College of Engineering
at the University of Kentucky

By

Rui He

Lexington, Kentucky

Director: Dr. David W. Herrin, Professor of Mechanical Engineering

Lexington, Kentucky

2015

ABSTRACT OF THESIS

AIRBORNE PATH FREQUENCY BASED SUBSTRUCTURING METHOD AND ITS APPLICATIONS

Frequency based substructuring (FBS) is routinely used to model structural dynamics. It provides a framework for connecting structural subsystems together, assessing path contributions, determining the effect of mount modification, and identifying inverse forces. In this work, FBS methods are extended to include acoustic subsystems and connecting pipes and ducts. Connecting pipes or ducts are modeled using the transfer matrix approach which is commonly used for modeling mufflers and silencers below the plane wave cutoff frequency. The suggested approach is validated using boundary element method (BEM) simulation. Applications of the procedure include determining airborne path contributions, the effect of treating ducts and apertures, and the effect of making lumped acoustic impedance modifications to a subsystem. The method can be simplified and used for determining the effect of design changes on the insertion loss of enclosures.

KEYWORDS: frequency based substructuring, airborne path, transfer path analysis, transfer matrix, noise control, mufflers silencers and partial enclosures

Rui He
Student's Signature

7th April, 2015
Date

AIRBORNE PATH FREQUENCY BASED SUBSTRUCTURING METHOD AND ITS APPLICATIONS

By

Rui He

Haluk E. Karaca
Director of Graduate Studies

May, 2015
Date

To my family and friends

ACKNOWLEDGEMENTS

I would like to first and foremost express my deepest gratitude to my advisor Professor David Herrin for his invaluable guidance and support, and for encouraging me to perform this work.

Sincere thanks also go to Professor Tim Wu and Professor John Baker, who serve as my committee members and provide helpful guidance in my research.

I would like to thank all my former and current colleagues, Huangxing Chen, Gong Cheng, Xin Hua, Quentin Hunsucker, Jiazhu Li, Wanlu Li, Jiawei Liu, Kangping Ruan, Shishuo Sun, Peng Wang, Yitian Zhang, and Limin Zhou. We had wonderful time during the study and research.

I would also thank my former roommates, Xingye Zhang and Wenwei Zeng who have helped me a lot both in academics and life.

Moreover, I would thank my bay area friends, especially my tennis partners, for having a colourful experience with joy.

Last but not the leat, I would thank my parents and falily for their continuous support and endless love.

TABLE OF CONTENTS

LIST OF TABLES

LIST OF FIGURES

Chapter 1

INTRODUCTION

1.1 Background

Industry is becoming increasingly concerned about the user experience when utilizing their products and services. One important concern is noise, vibration and harshness (NVH). In the automotive and heavy equipment industries, emphasis is placed on reducing structural vibration and interior cabin noise by a number of different strategies including isolation, damping treatments, and sound absorption. In the building industry, fan, compressor and flow noise impact the building environment and must be minimized. When it comes to the consumer electronics industry, low noise emissions from cell phone vibration, or from circuitry affect the user experience. Irrespective of the industry, reduction of noise is achieved by identifying noise sources, paths, and receivers and making appropriate changes.

Machines can be thought of as systems which consist of components and connections. Vibration or sound energy passes from active-side to passive-side components through connections. An active component consists of at least one source which may be vibrational or acoustic. For instance, an engine, compressor, or pump would be considered an active component. Passive components are driven by active components and include panels and windows, duct work and enclosures.

Structure-borne vibration propagates through mounts and isolators to the passive components. A receiver may be located on either an active or a passive

component. Receivers include the vibration or acoustic pressure at some specified position. Transfer functions relate the sources or inputs to the receivers or outputs. The response may be reduced by reducing the transfer function amplitude through proper isolation or damping, or by changing the transmission path through mass or stiffness modification.

Airborne paths are often the most important in buildings and partially enclosed sources. Noise propagates through air from the source to the receiver, and the transfer function is a function of geometry and noise control treatments. Chillers, boilers, furnaces, fans and pumps are common sources of noise in building environments. Sound energy propagates through the duct airspace from an equipment room to the other parts of the building. This airborne noise can be reduced by using sound absorbing materials like fiber or foam, adding silencers or plenums, or by extending the length of the ducts.

Similarly, partial enclosures are often used to reduce the transmission of noise from machinery to a receiver. The partial enclosure behaves like a barrier and normally includes sound absorption to reduce the noise within the enclosure itself. In that case, the enclosure compartment is analogous to the source room, and enclosure openings introduce airborne paths to the receiver.

Figure 1.1 engine-mount-body frameshows an engine mounted to an automobile frame and body. One important path is structure borne. The engine, which is the active component, is attached to the body frame through isolators or connections. The body frame is a passive component driven by the engine. Structural energy

propagates through the isolators to the frame and onto firewall which radiates sound to the passenger compartment.

Another important path can be classified as an airborne indirect path. The engine structure will radiate sound which will vibrate the firewall which in turn radiates sound to the passenger compartment. In this case, the engine compartment can be considered an active component, and the firewall and passenger compartments passive components.

Similarly, there is a path that can be classified as an airborne direct or strictly airborne path. The radiated noise in the engine compartment propagates to the receiver (i.e., driver) through any gaps or leaks between the engine and passenger compartments.

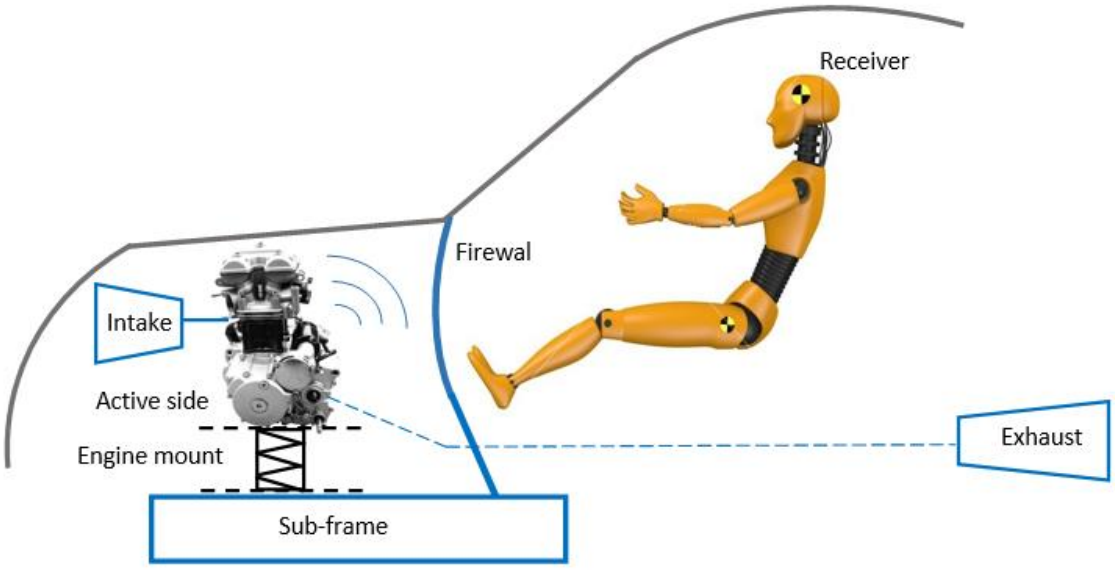

Figure 1.1 engine-mount-body frame

http://www.lmsintl.com/How-to-perform-transfer-path-analysis

An HVAC system is shown in Figure 1.2. The equipment room is the active component, and the building rooms are the passive components. Active and passive components are connected by ducts which are analogous to mounts for the mechanical system case. The direct airborne path is most important. Equipment generated noise passes through the ducts to the rooms. Another important path is the airborne indirect path. Noise within the ducts impinges on the ductwork which in turn radiates sound to the rooms. At low frequnecies, the structureborne path from the equipment vibration to the floors and walls may also be important.

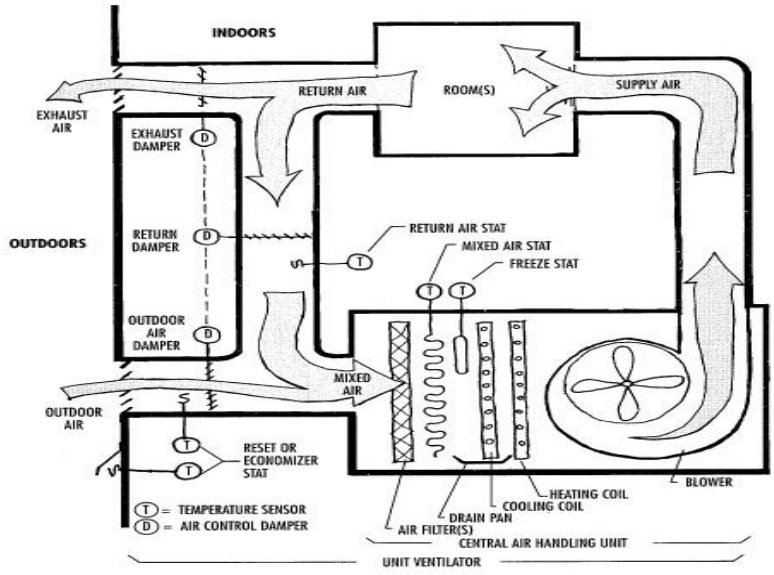

Figure 1.2 HVAC enclosures with pipes

http://www.epa.gov/iaq/schools/ventilationenergy.html

To identify the vibro-acoustic system response, frequency based substructuring (FBS, also referred to as Frequency Response Function (FRF) based

substructuring) is one of the most powerful methods in analyzing the responses of complex built-up structures. Frequency based substructuring is a transfer function based approach which can utilize both experimental or simulation results. It is assumed that the problem is linear and that transfer functions can be used to characterize the dynamic response of the vibro-acoustic system. Chapter 2 will provide a detailed review of FBS.

FBS is normally used in structure-borne mechanical system identification. The current work is aimed at extending FBS to include the modeling of airborne connections between subsystems. Examples include ducts, apertures, and leaks which are the direct analogs of isolators and springs in mechanical systems. Accordingly, the equations developed are similar to those used for the mechanical counterpart.

1.2 Objectives

In this work, FBS is used to characterize and simulate airborne paths. After a FBS representation is in place, airborne paths can be modified and the effects of modifications can be assessed. Specifically, the following objectives were accomplished:

- The FBS equations were developed for airborne paths and validated by boundary element simulation.
- The FBS approach was used to determine the contribution through airborne paths.

- The FBS approach was used to determine the effect of adding attenuation elements in the connecting ducts.
- The FBS approach was used to determine the response after lumped impedance modifications were made to airborne subsystems.
- FBS substructuring was utilized to determine the insertion loss of partial enclosures.

1.3 Organization

This thesis is organized in the following manner. Chapter 2 reviews the concepts of transfer path analysis (TPA) and frequency based substructuring in structure-borne systems. Mathematical models are introduced and methodology for measuring and modeling of systems is reviewed. After laying this groundwork, Chapter 3 derives the airborne system FBS, which is the basic theory.

Chapter 4 presents case-verifications of the airborne FBS theory derived in Chapter 3. Boundary element simulation is used for the case studies. Cases with two open pipes, two rooms and two sets of sources are described. The method is then simplified and utilized to predict the insertion loss of a partial enclosure.

In Chapter 5, an enclosure case experiment is presented to verify the airborne FBS theory. The sound pressure is predicted using FBS and compared with measurement.

Chapter 6 looks at applications of the approach. FBS is used to determine path contributions and to examine the effectiveness of adding muffler attenuation

elements to connecting ducts or making lumped impedance modifications to a subsystem.

Conclusions and recommendations for future work are discussed in Chapter 7.

Chapter 2

REVIEW OF FREQUENCY BASED SUBSTRUCTURING METHOD

Frequency based substructuring or FBS is an approach where a model of a system is developed based on transfer functions between inputs, outputs, and connections. The approach is sometimes called transfer path analysis (TPA) because transfer functions are sometimes referred to as paths. In this chapter, the method will be described and the assumptions will be detailed.

2.1 FBS background

Frequency based substructuring (FBS), which is sometimes referred to as FRF-based substructuring, is commonly used to rank structure-borne and airborne path contributions to a receiver. In general, models assume that the problem is linear and that transfer functions can be used to characterize the dynamic response of the vibro-acoustic system.

FBS was proposed by Jetmundsen et al. [1], who termed the procedure admittance modeling. Gordis et al. [2] derived the formulation for frequency domain structure synthesis. Avitabile [3], de Klerk et al. [4], and Craig Jr. [5] continued their work examining methods for making impedance modifications. In the intervening years, FBS has become quite popular in the experimental noise and vibration community.

There are several benefits to this approach. First, models can be developed using a combination of experimental and simulation tools. For example, complicated structural components like the engine and the transmission can be assessed experimentally while simpler components like the chassis and body-in-white can

be modeled using simulation. Thus, FBS provides a framework for integrating test and analysis information into a single model. Secondly, FBS provides a means for coupling components together in a system model. For a mechanical case, connections between subsystems via springs and rubber mounts can be modeled and system level effects can be understood. Moreover, different treatment options can be assessed without solving deterministic models of the entire system, greatly reducing computational time.

The work in this thesis is aimed at extending FBS to include the modeling of airborne connections between subsystems. Leaks, apertures, and ducts are direct analogs of isolators and springs in mechanical systems. Accordingly, FBS theory in acoustic systems is similar to that used for the mechanical counterpart.

2.2 Linear time invariant system

In order for FBS to be appropriate, it must be assumed that the system is linear time invariant. If the output $y(t)$ is a function of the input $x(t)$, it can be expressed as:

$$y(t) = \mathcal{H}\big(x(t)\big) \tag{2.1}$$

Time invariance is satisfied when a time shift σ applied to the input ($x(t)$ to $(t+\sigma)$) results in an equal shifted output ($y(t)$ to $(t+\sigma)$) [6]. This can be expressed as:

$$y(t+\sigma) = \mathcal{H}\big(x(t+\sigma)\big)\forall\sigma \tag{2.2}$$

Linearity implies that if the output will be scaled by the same amount as the input. Thus,

$$\mathcal{H}\big(\alpha u(t) + \beta v(t)\big) = \alpha\mathcal{H}\big(u(t)\big) + \beta\mathcal{H}\big(v(t)\big) \tag{2.3}$$

Moreover, the principle of superposition must also be valid. This means that the outputs from different inputs can be determined separately and then superimposed. It reflects the parallel connections of the linear time invariant (LTI) system. Accordingly, the output to input relationship can be modeled using the block diagram shown in Figure 2.1. This is expressed as:

$$y(t) = \mathcal{H}\big(x(t)\big) = \sum_{m=1}^{n} \mathcal{H}_m\big(x(t)\big) \tag{2.4}$$

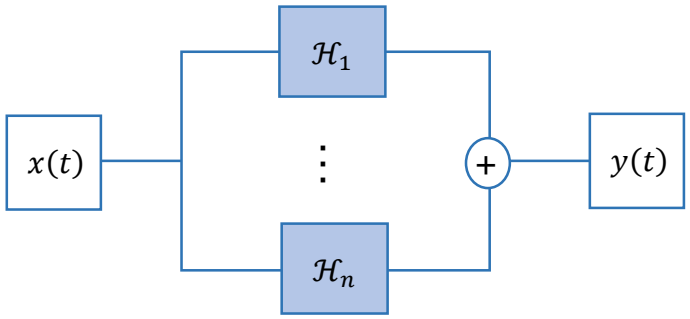

Figure 2.1 Schematic of an LTI system in parallel

2.3 Transfer function of second order system

A second order ordinary differential equation can describe most mechanical systems at low frequencies. A single degree of freedom system is shown in Figure 2.2. The equation of motion can be found using Newton's laws of motion and expressed as:

$$M\ddot{x}(t) + C\dot{x}(t) + Kx(t) = F(t) \tag{2.5}$$

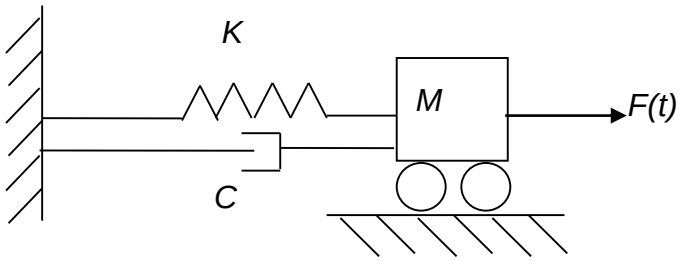

Figure 2.2 SDOF dynamics system

where $x(t)$ is the displacement. $M, C, \text{and } K$ represent the mass, damping and stiffness respectively. $F(t)$ is the external applied force to the system and is assumed to be harmonic. For the single degree of freedom (SDOF) system shown above, its undamped natural frequency ω_n and damped natural frequency ω_d are expressed as:

$$\omega_n = \sqrt{\frac{K}{M}} \tag{2.6}$$

and

$$\omega_d = \omega_n\sqrt{1-\xi^2} \tag{2.7}$$

where

$$\xi = \frac{C}{2\sqrt{KM}} \tag{2.8}$$

When the system consists of multiple degrees of freedom (MDOF), a matrix system of equations can be expressed as:

$$\mathbf{M}_{n\times n}\ddot{x_n}(t) + \mathbf{C}_{n\times n}\dot{x_n}(t) + \mathbf{K}_{n\times n}x_n(t) = F_n(t) \tag{2.9}$$

where $\mathbf{M}_{\mathrm{n}\times\mathrm{n}}$, $\mathbf{C}_{\mathrm{n}\times\mathrm{n}}$, and $\mathbf{K}_{\mathrm{n}\times\mathrm{n}}$ are the respective mass, damping, and stiffness matrices for an n degree of freedom system. $\mathbf{M}_{\mathrm{n}\times\mathrm{n}}$, $\mathbf{C}_{n\times n}$, and $\mathbf{K}_{n\times n}$ are symmetric, and $\mathbf{M}_{n\times n}$ is diagonal. This is the case when masses are "point lumped" at the DOF locations.

For Rayleigh or proportional damping, the damping matrix can be expressed as a superposition of the mass and stiffness matrices and can be expressed as $\mathbf{C} = \alpha\mathbf{M} + \beta\mathbf{K}$. For a single degree of freedom system, the transfer function can be expressed in the Laplace domain as:

$$\frac{X(s)}{F(s)} = \frac{\omega_n^2}{s^2 + 2\xi\omega_n s + \omega_n^2} \tag{2.10}$$

When expressed in terms of eigenvectors in modal space, the FRF can be written as:

$$H(j\omega) = \sum_{i=1}^{n} \frac{\{\Phi_{\mathrm{i}}\}\{\Phi_{\mathrm{i}}\}^{\mathrm{T}}}{(\omega_i^2 - \omega^2) + j2\xi_i\omega_i\omega} \tag{2.11}$$

where $\{\Phi_{\mathrm{i}}\}$ is the i^{th} order mode shape, and ω_i is the natural frequency of the ith degree of freedom [7]. The transfer function between the input and output of the system represents the fundamental characteristics of the system, and is independent of the input depending instead on the structure and path between the input and response positions. The transfer function is sometimes referred to as a path and is the key to transfer path analysis.

2.4 FBS theory and application

2.4.1 FBS theory review

Transfer Path Analysis (TPA) is commonly used to identify dominant paths and then determine appropriate treatments in complicated systems. The system is normally broken up into active and passive components. The former containing the sources, and the latter containing the receivers where the responses are measured. The classical “source - path – receiver” transfer path model shown in Figure 2.3 FBS model, which was first suggested in the 1950’s [8], and was enhanced to become frequency based substructuring in the 1980’s [9, 10]. The basic ideas and some applications are now discussed.

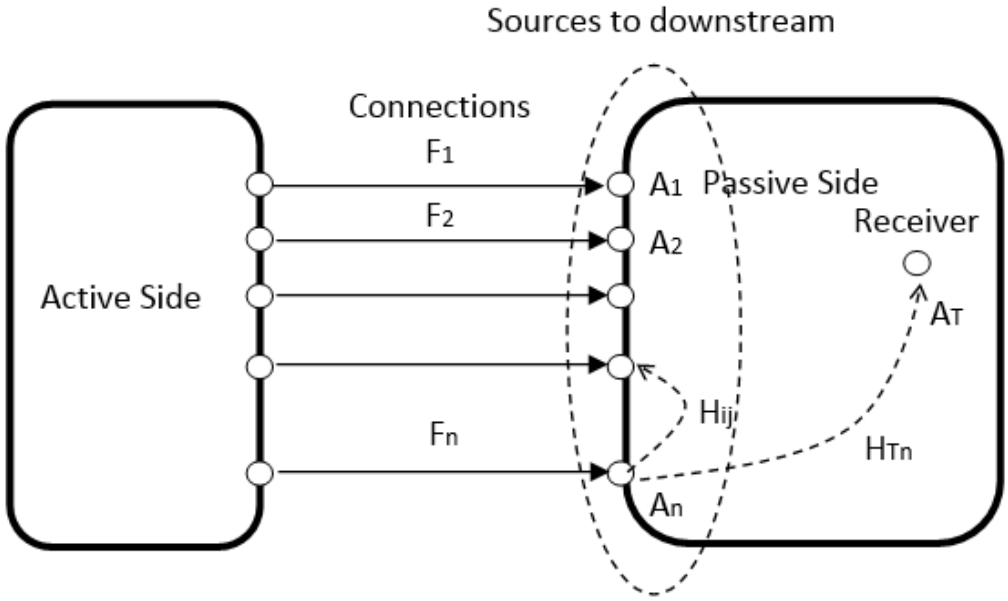

Figure 2.3 General TPA model

Each connection point in the FBS model will generate a response at all other connection points and receivers as shown in Figure 2.3 for the passive side. These

input-output relationships are expressed as frequency response functions (FRF's) and are sometimes called noise transfer functions (NTF's). The paths between sources and receivers are represented by these FRF's. The contribution of a single path to a response point can be determined by multiplying the FRF for a path by a corresponding input. Since linear time invariance is assumed, the response is assumed to result from the contribution from each respective input.

The system response can be described as the superposition of structureborne (y_{ri}) and airborne (y_{rj}) responses. Accordingly,

$$y_r = \sum_{i=1}^{n} y_{ri} + \sum_{j=1}^{m} y_{rj} \tag{2.12}$$

The structureborne response can be expressed in terms of the input forces (F_i) and the transfer function relating the force to the response (H_{ri}).

$$y_{ri} = H_{ri} \times F_i \tag{2.12a}$$

The transfer function H_{ri} can be determined from

$$H_{ri} = \left.\frac{y_r}{F_i}\right|_{F_k=0, k\neq i} \tag{2.12b}$$

The airborne response can be expressed in terms of the acoustic source volume velocity (Q_j) and transfer functions relating the acoustic source to the response (H_{rj}) as

$$y_{rj} = H_{rj} \times Q_j \tag{2.12c}$$

where the transfer functions are determined using

$$H_{rj} = \left.\frac{y_r}{Q_j}\right|_{Q_p=0, p\neq j} \tag{2.12d}$$

Note that all transfer functions are determined with one source active and all other connections removed.

There are several procedures to obtain frequency response (or transfer) functions. They can be determined numerically using finite or boundary element analysis. On the other hand, frequency response functions could be measured directly or indirectly via measurement. An impact hammer or shaker is usually used as the source for structural paths. For acoustic transfer functions, a volume velocity source (often a loudspeaker) must be used. The response is collected using accelerometers (vibration) or microphones (sound pressure).

However, direct measurements are sometimes difficult due to loads applied at difficult to reach positions (i.e., positions internal to a machine). In that case, transfer functions can be measured easier by swapping the source and response and taking advantage of reciprocity [11]. In most cases, placing a source (which has a sizeable footprint) at a receiver location which is easily accessible is preferable. Measurements are then procured at the source locations. Another advantage of this approach is that there are often less receiver points of interest than sources. It is normally more convenient to move sensors or acquire data simultaneously at a number of sensors than it is to move the more massive source.

Systems are often highly coupled and excitation at one source will produce vibration at other sources. It is important to measure the FRF's for each source

separately while avoiding cross contamination from the other sources. As in Equations 2.12c and 2.12d, frequency response functions should be procured with all other sources inactive. Failure to uncouple the other sources will lead to errors. Transfer path analysis works especially well at low frequencies. Plunt [12] provides a good overview of TPA discussing both low and high frequency predictions.

Sometimes transfer functions are estimated where an acceleration response is measured instead of an input since inputs are difficult to measure. This is often referred to as operational transfer path analysis. Alternatively, hybrid models can be used where both measured and simulated transfer functions are used [13, 14, 15]. The aforementioned approaches can significantly speed up the process but the accuracy may be compromised.

2.4.2 FBS applications

FBS is useful for a number of applications [16, 17]. The dynamic forces during machinery operation are typically difficult to measure. In that case, the response can be measured at a number of easily accessible sensor locations. Transfer functions between the force and sensor locations can be measured with the system off. The unknown forces can then be determined by matrix inversion. The first step of the method is to collect the frequency response functions between each source, and indicators and receivers. Indicators are response points at passive locations. Paths or frequency response functions are measured or determined computationally between each source and indicator. A transfer function matrix is then populated using the determined transfer functions. After

which, the responses are measured at the indicators and receivers during operating conditions. Operational or inverse loads can be determined using:

$$\begin{bmatrix} F_1 \\ F_2 \\ \vdots \\ F_n \end{bmatrix} = \begin{bmatrix} H_{11} & H_{12} & \dots & H_{1n} \\ H_{21} & H_{22} & \dots & H_{2n} \\ \vdots & \vdots & \ddots & \vdots \\ H_{m1} & H_{m2} & \cdots & H_{mn} \end{bmatrix}^{-1} \begin{bmatrix} A_1 \\ A_2 \\ \vdots \\ A_m \end{bmatrix} \tag{2.13}$$

The number of measured indicator responses should exceed the number of unknown loads to be calculated in order to insure that the problem is well-conditioned. Accordingly, m should be greater than n. Then unknown forces can be determined using a least squares solution [18]. It is recommended that $m \geq 2n$ to minimize ill-conditioning problems when calculating the pseudo-inverse [19].

Path contribution analysis is another widely used application. The contribution from each path to the receiver is calculated by multiplying the FRF and the corresponding load. This can be expressed equationally as:

$$y_{ri} = H_{ri} \times F_i \tag{2.14}$$

If the loads are known, the primary source contributions can be identified. The results are commonly shown in a path contribution plot, like in Figure 2.4 where the path contributions are shown as a function of frequency and/or RPM. From Figure 2.4, it can be seen that the major contribution comes from Paths 3 and 4 at 3500 RPM. Gajdatsy [20] discusses the limitations of a path contribution plot. This particular plot does not show the phase and does not illustrate cancellation effects which may be important at low frequencies.

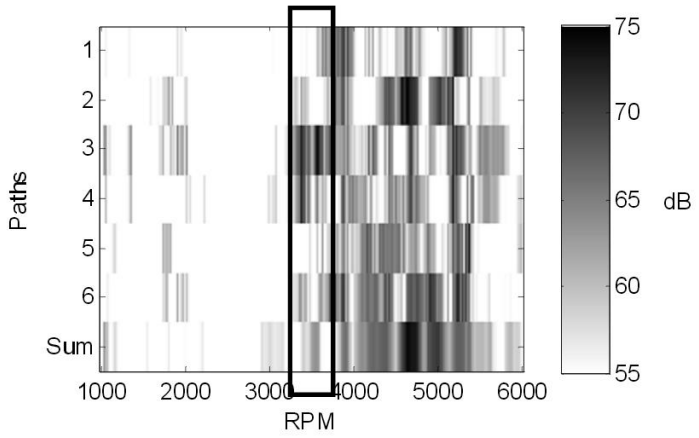

Figure 2.4 Example of path contribution plot [20]

Flexible connections like mounts are often used to decouple active from passive components [21, 22]. If the mass of the connection is neglected, forces are equal on opposite sides of the mounts. The connector can be modeled as a complex dynamics stiffness which includes both stiffness and damping. This dynamic stiffness may be frequency dependent and may be expressed as:

$$F_i(\omega) = K_i(\omega) \times \frac{a_{ai}(\omega) - a_{pi}(\omega)}{-\omega^2} \tag{2.15}$$

$F_i(\omega)$ is the mount force, $K_i(\omega)$ the stiffness of mount and $a_{ai}(\omega)$ and $a_{pi}(\omega)$ are active and passive side acceleration respectively.

2.5 Summary

In this chapter, the prior work and assumptions for transfer path analysis have been reviewed. It has been shown that the method is advantageous for determining inverse forces, path contributions, and for predicting the effect of connection modifications. The next chapter will extend the method to airborne path analysis including airborne connections.

Chapter 3

DEVELOPMENT OF FREQUENCY BASED SUBSTRUCTURING FOR AIRBORNE PATHS

This Chapter will detail the mathematics of FBS for structure-borne paths. After which, the theory will be extended to airborne paths in which connections are modeled using transfer matrix theory.

3.1 System modeling using frequency based substructuring

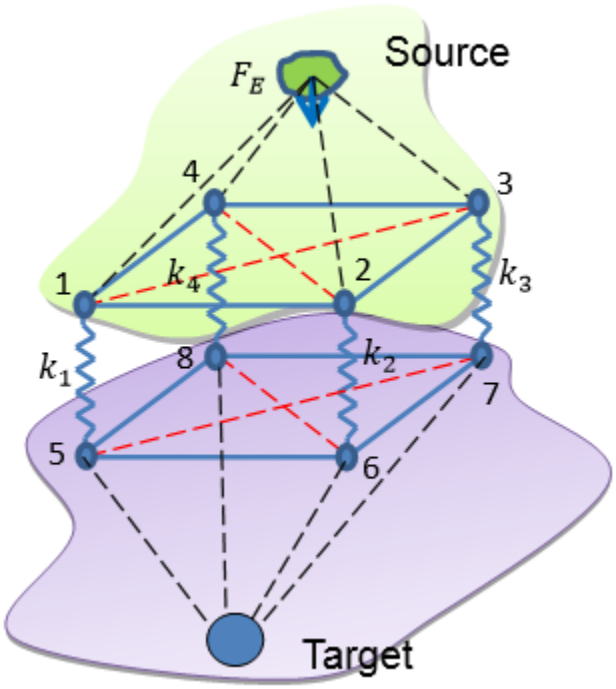

Figure 3.1 Four-spring mount system

A simple four-spring mount system case is discussed to demonstrate the FBS concepts. Figure 3.1 shows a dynamic system containing active (i.e., source side) and passive (i.e., target side) components with four springs as connections in between the active and passive components.

Sources might include internal combustion engines or compressors. Assume the source can be represented by a single load F_E to the system.

The response at the active and passive side connection points can be expressed in matrix form as:

$$\begin{bmatrix} x_1 \\ x_2 \\ x_3 \\ x_4 \end{bmatrix} = \begin{bmatrix} H_{11} & H_{12} & H_{13} & H_{14} \\ H_{21} & H_{22} & H_{23} & H_{24} \\ H_{31} & H_{32} & H_{33} & H_{34} \\ H_{41} & H_{42} & H_{43} & H_{44} \end{bmatrix} \begin{bmatrix} F_1 \\ F_2 \\ F_3 \\ F_4 \end{bmatrix} + \begin{bmatrix} H_{1E} \\ H_{2E} \\ H_{3E} \\ H_{4E} \end{bmatrix} F_E \tag{3.1}$$

and

$$\begin{bmatrix} x_5 \\ x_6 \\ x_7 \\ x_8 \end{bmatrix} = \begin{bmatrix} H_{55} & H_{56} & H_{57} & H_{58} \\ H_{65} & H_{66} & H_{67} & H_{68} \\ H_{75} & H_{76} & H_{77} & H_{78} \\ H_{85} & H_{86} & H_{87} & H_{88} \end{bmatrix} \begin{bmatrix} F_5 \\ F_6 \\ F_7 \\ F_8 \end{bmatrix} \tag{3.2}$$

respectively where F_i are the forces applied at the connection points and H_{ij} are the transfer functions between connection points. Note that the forces are defined along the axis of the spring in this particular case but forces (or torques) may be considered in all six degrees of freedom at each point if needed. The two equations can be combined as:

$$\begin{bmatrix} x_1 \\ \vdots \\ x_4 \\ x_5 \\ \vdots \\ x_8 \end{bmatrix} = \begin{bmatrix} H_{11} & H_{12} & H_{13} & H_{14} & & 0 & \\ H_{21} & H_{22} & H_{23} & H_{24} & & & \\ H_{31} & H_{32} & H_{33} & H_{34} & & & \\ H_{41} & H_{42} & H_{43} & H_{44} & & & \\ & & 0 & & H_{55} & H_{56} & H_{57} & H_{58} \\ & & & & H_{65} & H_{66} & H_{67} & H_{68} \\ & & & & H_{75} & H_{76} & H_{77} & H_{78} \\ & & & & H_{85} & H_{86} & H_{87} & H_{88} \end{bmatrix} \begin{bmatrix} F_1 \\ \vdots \\ F_4 \\ F_5 \\ \vdots \\ F_8 \end{bmatrix} + \begin{bmatrix} H_{1E} \\ H_{2E} \\ H_{3E} \\ H_{4E} \\ 0 \\ 0 \\ 0 \\ 0 \end{bmatrix} F_E \tag{3.3}$$

For a certain spring mount, the relationship between the upper and lower positions can be expressed through a transfer or transmissibility matrix, which is a characteristic property of the mount. This can be expressed as:

$$\begin{bmatrix} x_i \\ F_i \end{bmatrix} = [T] \begin{bmatrix} x_{i+4} \\ F_{i+4} \end{bmatrix} \tag{3.4}$$

If all connections are included, a connection matrix can be defined as:

$$\begin{bmatrix} x_1 \\ \vdots \\ x_4 \\ x_5 \\ \vdots \\ x_8 \end{bmatrix} = [T^*] \begin{bmatrix} F_1 \\ \vdots \\ F_4 \\ F_5 \\ \vdots \\ F_8 \end{bmatrix} \tag{3.5}$$

where $[T^*]$ is the combined matrix and is reconfigured from the $[T]$ matrix for each mount.

The response at a receiver on the passive side can be obtained by:

$$x_T = H_{T5}F_5 + H_{T6}F_6 + H_{T7}F_7 + H_{T8}F_8 \tag{3.6}$$

It is common to solve for either the unknown forces $[F_i]$ or responses $[x_i]$ using Equation 3.3. Once the unknown forces are known, the response at the target can be identified. Additionally, each of the terms on the right hand side of Equation 3.6 is the contribution of a single force to the response.

Transfer path analysis (TPA) has been applied to airborne paths to determine the contributions at receiver locations. In most cases, transfer functions are measured for the reciprocal case [24] and the volume velocity is measured for patches on the surface using either acceleration or sound intensity measurements [23, 24]. This approach is commonly referred to as panel contribution analysis.

In this work, FBS will be applied to airborne paths for interior acoustic spaces attached by ducts. Transfer matrix theory is utilized to simulate the connections between larger airspaces. The approach described is beneficial for determining the effect of adding treatments in connecting ducts.

3.2 Frequency based substructuring for airborne paths

In the discussion that follows, the equations are derived for the two-room and two-opening case shown in Figure 3.2. The two airborne pathways are denoted as connections 1 and 2. The source and receiving sides of the ducts are denoted as a and b respectively (See Figure 3.2). First, assume that Room a is closed and sources are placed at the openings. The sound pressure at the entry to Connection 1 will be the summation from the source itself plus the contributions from each of the openings. In that case, the sound pressure at the entry to connection 1 (p_1^a) can be expressed as

$$p_1^a = P_1^a + H_{11}^a S_1 u_1^a + H_{12}^a S_2 u_2^a \tag{3.7}$$

The first term on the right hand side of Equation 3.7 is the sound pressure from the source assuming that connection 1 is closed. It can be found via analysis provided the source is well understood. Alternatively, it can be determined experimentally by sealing the room. The remaining terms on the right hand side are the contributions from openings 1 and 2 (side a).

A similar expression can be also written for the sound pressure at the entry to airborne pathway 2 (p_2^a). That can be expressed as:

$$p_2^a = P_2^a + H_{21}^a S_1 u_1^a + H_{22}^a S_2 u_2^a \tag{3.8}$$

Similarly, the first term on the right hand side is the blocked sound pressure which is denoted as P_2^a. Expressions can also be developed which relate the particle velocity and sound pressure at the openings for side b. Accordingly,

$$p_1^b = H_{11}^b S_1 u_1^b + H_{12}^b S_2 u_2^b \tag{3.9a}$$

$$p_2^b = H_{21}^b S_1 u_1^b + H_{22}^b S_2 u_2^b \tag{3.9b}$$

For connections between subsystems, the sound pressure and particle velocity on side a can be related to that on side b using transfer matrix theory. This is mathematically expressed as

$$\begin{Bmatrix} p_i^a \\ S_i u_i^a \end{Bmatrix} = \begin{bmatrix} A_i & B_i \\ C_i & D_i \end{bmatrix} \begin{Bmatrix} p_i^b \\ S_i u_i^b \end{Bmatrix} \tag{3.10}$$

where i denotes the acoustic connection or pathway. Equation 3.10 can be rearranged and expressed as

$$\begin{Bmatrix} p_i^a \\ p_i^b \end{Bmatrix} = \begin{bmatrix} a_i & b_i \\ c_i & d_i \end{bmatrix} \begin{Bmatrix} S_i u_i^a \\ S_i u_i^b \end{Bmatrix} \tag{3.11}$$

where

$$a_i = \frac{A_i}{C_i}$$

$$b_i = B_i - \frac{A_i D_i}{C_i}$$

$$c_i = \frac{1}{C_i} \tag{3.12}$$

$$d_i = -\frac{D_i}{C_i}$$

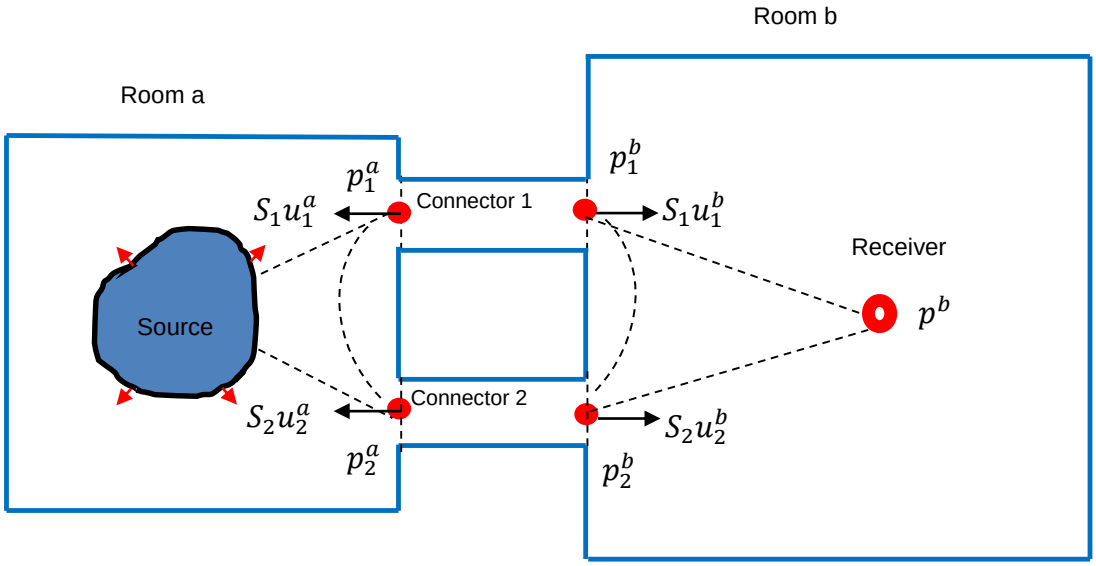

Figure 3.2 Schematic showing acoustics systems

Equations 3.7, 3.8, and 3.9 can be expressed in matrix form as

$$\begin{Bmatrix} p_1^a \\ p_2^a \\ p_1^b \\ p_2^b \end{Bmatrix} = \begin{bmatrix} H_{11}^a & H_{12}^a & 0 & 0 \\ H_{21}^a & H_{22}^a & 0 & 0 \\ 0 & 0 & H_{11}^b & H_{12}^b \\ 0 & 0 & H_{21}^b & H_{22}^b \end{bmatrix} \begin{Bmatrix} S_1u_1^a \\ S_2u_2^a \\ S_1u_1^b \\ S_2u_2^b \end{Bmatrix} + \begin{Bmatrix} P_1^a \\ P_2^a \\ 0 \\ 0 \end{Bmatrix} \tag{3.13}$$

which is analogous to Equation 3.3 for the structural case.

For the case with two connections, Equation 3.11 can be expanded as

$$\begin{Bmatrix} p_1^a \\ p_2^a \\ p_1^b \\ p_2^b \end{Bmatrix} = \begin{bmatrix} a_1 & 0 & b_1 & 0 \\ 0 & a_2 & 0 & b_2 \\ c_1 & 0 & d_1 & 0 \\ 0 & c_2 & 0 & d_2 \end{bmatrix} \begin{Bmatrix} S_1 u_1^a \\ S_2 u_2^a \\ S_1 u_1^b \\ S_2 u_2^b \end{Bmatrix} \tag{3.14}$$

which is the analog to Equation 3.5 for the structural case.

Equations 3.12 and 3.13 can then be solved for the volume velocities ($S_i u_i^j$). Thus, the equation can be rewritten as:

$$\begin{Bmatrix} S_1 u_1^a \\ S_2 u_2^a \\ S_1 u_1^b \\ S_2 u_2^b \end{Bmatrix} = \left(\begin{bmatrix} a_1 & 0 & b_1 & 0 \\ 0 & a_2 & 0 & b_2 \\ c_1 & 0 & d_1 & 0 \\ 0 & c_2 & 0 & d_2 \end{bmatrix} - \begin{bmatrix} H_{11}^a & H_{12}^a & 0 & 0 \\ H_{21}^a & H_{22}^a & 0 & 0 \\ 0 & 0 & H_{11}^b & H_{12}^b \\ 0 & 0 & H_{21}^b & H_{22}^b \end{bmatrix} \right)^{-1} \begin{Bmatrix} P_1^a \\ P_2^a \\ 0 \\ 0 \end{Bmatrix} \tag{3.15}$$

For the general case involving sources in multiple rooms and multiple connection paths, this can be rewritten as:

$$\{Su\} = ([T] - [H])^{-1}\{P\} \tag{3.16}$$

where $[T]$ and $[H]$ are matrices for connections and subsystems respectively and $\{Su\}$ and P are vectors for the volume velocities and blocked sound pressures respectively.

Once the volume velocities are obtained, the sound pressures at a receiver point in rooms a and b can be found via

$$p^a = H_{a1} S_1 u_1^a + H_{a2} S_2 u_2^a + P^a \tag{3.17a}$$

and

$$p^b = H_{b1}S_1u_1^b + H_{b2}S_2u_2^b \tag{3.17b}$$

respectively.

3.3 Transfer function determination

The transfer functions (H_{ij}) relating the sound pressure at one opening to the volume velocity at another (or the same) are easily determined using acoustic simulation. In order to determine the transfer functions, a unit velocity is defined as a boundary condition at one opening with other openings sealed (i.e., rigid) and the source inactive. In all equations, it is assumed that a positive volume velocity is directed into the room (i.e., acoustic subdomain).

Transfer functions can also be determined experimentally. This is most easily accomplished by attaching an impedance tube (a tube with a loudspeaker on one side) at an opening. The volume velocity at the end of the tube can be found by measuring the sound pressure at two points inside the tube. Using wave decomposition, the volume velocity at the end of the opening of the tube can be expressed as (variables are defined in Fig A.1 in Appendix A):

$$u_0 = \frac{S_0|p_1|}{\rho c(R+1)}(e^{-jkL_1} - Re^{jkL_1}) \tag{3.18}$$

3.4 Transfer matrix models for airborne connections

The connection elements in acoustic systems can consist of straight pipes, perforated panels, Helmholtz resonators and other acoustic elements. Plane wave

behavior is assumed in the acoustic connections (i.e., sound pressure is constant for any cross-section).

The sound pressure and volume velocity at the inlet and outlet for several different connections are summarized. For a straight pipe, the transfer matrix can be expressed as:

$$\begin{Bmatrix} p_1 \\ S_1 u_1 \end{Bmatrix} = \begin{bmatrix} \cos kL & \frac{j\rho c}{S_2}\sin kL \\ \frac{jS_1}{\rho c}\sin kL & \frac{S_1}{S_2}\cos kL \end{bmatrix} \begin{Bmatrix} p_2 \\ S_2 u_2 \end{Bmatrix} \tag{3.19}$$

Figure 3.3 schematic of the variables and the sign convention for volume velocity

Elements such as quarter wave tubes or Helmholtz resonators can be modeled as a parallel or branch impedance. The transfer matrix can be expressed as:

$$T = \begin{bmatrix} 1 & 0 \\ Z_B & 1 \end{bmatrix} \tag{3.20}$$

An example of a parallel or branch impedance is a closed side branch (i.e. quarter wave tube). The acoustic impedance can be expressed as:

$$Z_B = -\frac{j\rho c}{S_B}\cot(kL_B) \tag{3.21}$$

where L_B and S_B are the length and cross-sectional area of the closed side branch respectively [7]. Similarly, the branch impedance of a Helmholtz resonator is

$$Z_b = -j\left(\frac{\rho\omega L'}{S_B} - \frac{1}{\omega}\frac{\rho c^2}{V}\right) \tag{3.22}$$

where L' is the equivalent length of the neck, V is the volume of the resonator and S_B is the area of the side branch [7].

Elements can be cascaded in series as shown in Figure 3.4. The total transfer matrix can be expressed as:

$$[T] = [T_1][T_2] \dots [T_N] \tag{3.23}$$

for N elements.

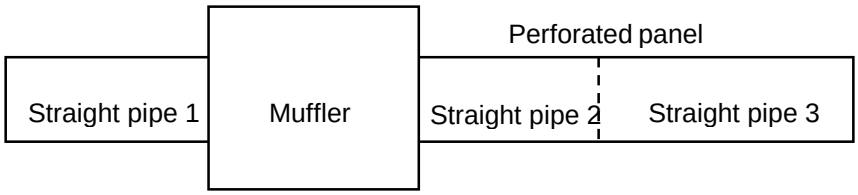

Figure 3.4 Duct with a number of elements

Note that the sign convention for volume velocity is reversed in Equations 3.10-3.12. Thus, the four pole parameters in Equation 3.10 can be expressed in terms of $[T]$ in Equation 3.23 as:

$$\begin{bmatrix} A & B \\ C & D \end{bmatrix} = \begin{bmatrix} T_{11} & T_{12} \\ -T_{21} & -T_{22} \end{bmatrix} \tag{3.24}$$

Notice that the signs of matrix elements (2, 1) and (2, 2) have been reversed.

3.5 Insertion loss prediction

Insertion loss is defined as the radiated sound pressure or sound power change due to the insertion of attenuation elements. It is often used to evaluate how well an attenuation device will perform in the actual system. The insertion loss for an enclosure can be defined as the difference between two sound pressure levels at the same point without and with the enclosure. It can also be defined as the reduction in radiated sound power due to the enclosure.

The termination impedance at the duct opening can be determined using the formulas for unflanged and flanged openings [25, 72, 73]. The termination impedance of an unflanged opening can be expressed as:

$$Z_{rad} = \frac{\rho c(1+R)}{S(1-R)} \tag{3.25}$$

where ρ is the density of air, c the speed of sound in air and S the cross-sectional area of the opening. R denotes the reflection coefficient which can be expressed as:

$$R = -R_0 e^{-j2k\alpha\zeta_0} \tag{3.26}$$

where k is the wave number and α the radius of the opening. ζ_0 is the end correction which is:

$$\zeta_0 = \begin{cases} 0.6133 - 0.1169(ka)^2, & ka < 0.5 \\ 0.6393 - 0.1104ka, & 0.5 \leq k < 2 \end{cases} \tag{3.27}$$

R_0 is the amplitude of the reflection coefficient without flow and can be expressed as:

$$R_0 = 1 + 0.01336ka - 0.59079(ka)^2 + 0.33576(ka)^3 - 0.06432(ka)^4, ka < 1.5 \quad (3.28)$$

In a similar manner, the termination impedance for a flanged opening can be written as:

$$Z_{rad} = \frac{\rho c}{S}(R_1 - jX_1) \quad (3.29)$$

where

$$R_1 = 1 - \frac{J_1(2ka)}{ka} \quad (3.29a)$$

and

$$X_1 = \frac{H_1(2ka)}{ka} \quad (3.29b)$$

J_1 and H_1 are the first order Bessel function of first kind and Struve function of first kind respectively.

Given the transfer functions, partial pressures from the sources and the transfer matrix of the connections, the sound pressure and volume velocity at the openings can be determined by solving the Equations 3.16. The sound pressure at the receiver positions can be determined using Equation 3.17.

The sound intensity can be determined using the previously calculated sound pressure and volume velocity. Accordingly, the radiated sound power from the openings can be obtained by [26]:

$$W = \sum_{i=1}^{N} \frac{1}{2} \mathrm{Re}(P_i Q_i^*) \tag{3.30}$$

The sound power of a source can be found by integrating the normal component of the mean active sound intensity over any closed contour *S* which encloses the sound source [27]. The sound power is expressed as:

$$W_S = \int_S \bar{I_n}\, dS \tag{3.31}$$

The mean active intensity can be found from:

$$\bar{I_a} = \overline{pu} = \frac{1}{2} Re\{\tilde{p}\tilde{u}^*\} \tag{3.32}$$

Here $\tilde{\mathrm{p}}$ and $\tilde{u}$ contain the space-dependent terms.

The estimated sound power can be determined by 1) estimating the normal component of the mean active intensity at *N* fixed field points on any surface enclosing the source; and 2) weighting with the corresponding area. The sound power can be determined by summing up the intensities and respective areas using:

$$W_S \approx \sum_{i=1}^{N} \overline{I_{nl}}\, \Delta S_i \tag{3.33}$$

3.6 Summary

In this chapter, frequency based substructuring was implemented for airborne paths with connections between airspaces described via transfer matrix theory. This approach is especially applicable to heating, ventilation, and air conditioning systems in which rooms are connected by ducts which may be treated or untreated. A definition of insertion loss for enclosures is also presented. With the theoretical foundation in place, the next chapter presents numerical cases which validate the theory.

Chapter 4

VALIDATION OF FREQUENCY BASED SUBSTRUCTURING APPROACH

In the prior chapter, a frequency based substructuring (FBS) approach for dealing with air spaces with connecting ducts was detailed. In this chapter, the approach is validated using the boundary element method. The 3-D modeling software Pro-Engineer (Creo) was used to build the geometry of the enclosure, and ANSYS was used to generate the mesh of the geometry. The software LMS Virtual.Lab was used for all boundary element analyses.

4.1 Sound pressure prediction

4.1.1 Two rooms, two connecting pipes

The first validation case consists of two rooms connected by two pipes. A source is placed in Room a. Figure 4.1 shows a schematic of the model. The two rooms are treated as two separate subsystems and the two pipes are modeled as connections. Each opening can be considered as a connection point. Accordingly, a connecting duct is analogous to a structural mount and a connection point to one side of a mount. The objective is to compare the response using a BEM model of the complete system with the calculated result using FBS.

Figure 4.2 shows the BEM model. The indirect boundary element method was used for the analysis [27]. Table 4.1 shows the dimensions of the two rooms. The length and diameter of the connecting pipes are 0.5 m and 0.1 m respectively. The positions and strengths of the sources located in Room a are shown in Table 4.2. A response or field point was positioned in Room b at the position of (0.3, 0.2, 1.1) (unit: m). The connections are located in Room b at the positions of (-0.2, -0.2,

0.85) (unit: m) and (-0.33, -0.03, 0.85) (unit: m) respectively. The fluid inside the rooms is assumed to be air with a speed of sound and density of 340 m/s and 1.225 kg/m^3 respectively. There are 5173 nodes and 5174 elements in the model with the element edge length 0.05 m. The model is valid up to the frequency range of 1000 Hz.

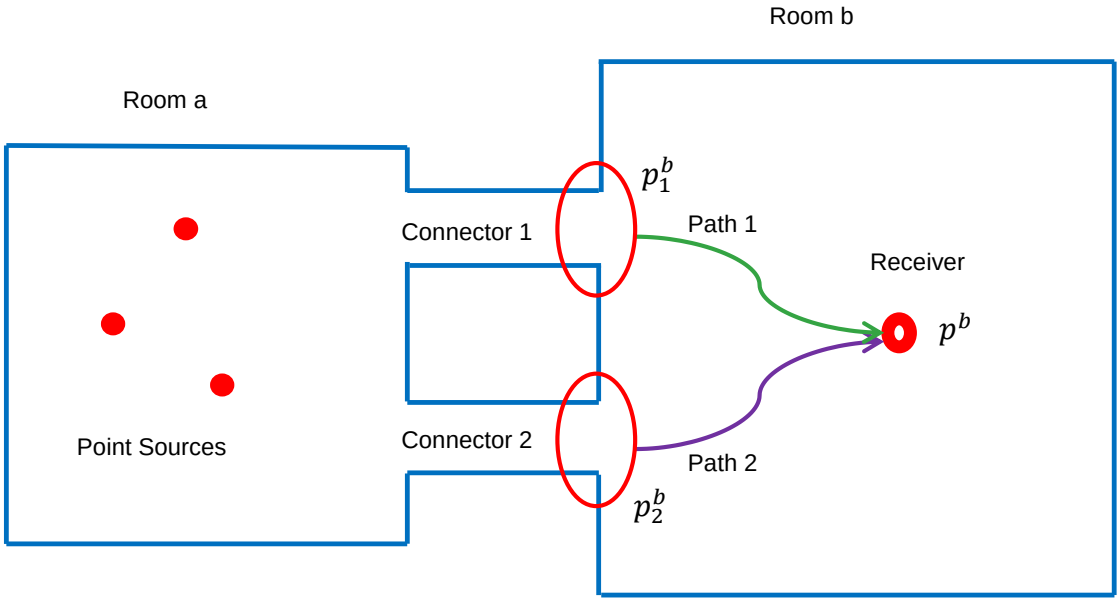

Figure 4.1 Schematic of two-room validation case

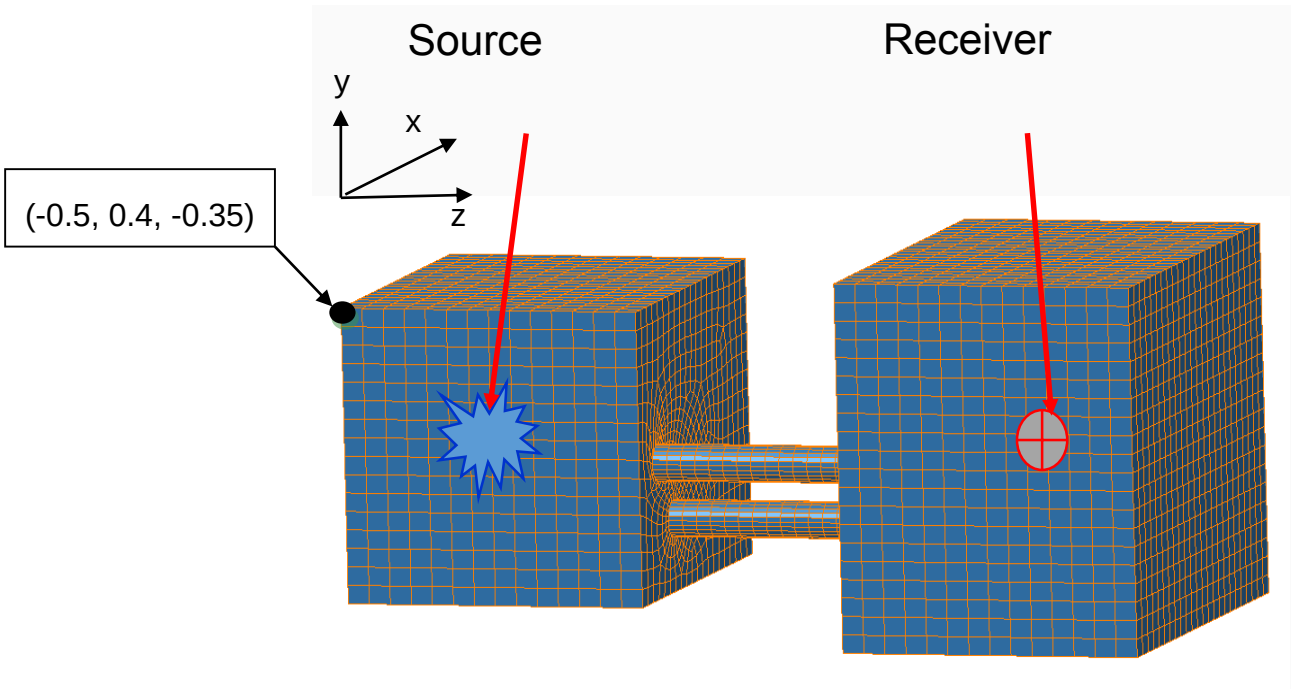

Figure 4.2 BEM model of two-room validation case

Table 4.1 Dimensions of rooms

Room No.	*Length (Lz) m*	*Width (Lx) m*	*Height (Ly) m*
a	0.7	1.0	0.8
b	0.7	1.2	1.0

Table 4.2 Positions and strength of the sources in Room a.

Monopole source	*x position m*	*y position m*	*z position m*	*Strength*	
				Real (kg/s2)	*Image (kg/s2)*
1	-0.30	0	0	1	0
2	0.20	-0.20	0.20	1	0
3	0.28	0.22	-0.10	1	0

4.1.1.1 Step 1: Determine transfer functions

The transfer functions were calculated using the method discussed in the Section 3.3. In the discussion that follows, a direction of sound propagation was assumed from the source to the receiver room. Note that the method does not require the direction of propagation to be known. Four separate BEM runs (one for each opening in each component) were required to define all of the required transfer functions. In each run, a unit velocity was applied on the opening and was directed into the acoustic domain of the respective airspace with the other opening blocked. The sound pressures at the two openings were obtained to calculate the transfer functions as shown in Figure 4.3. The receiver transfer functions should also be determined in the passive-side component. See Figure 4.4.

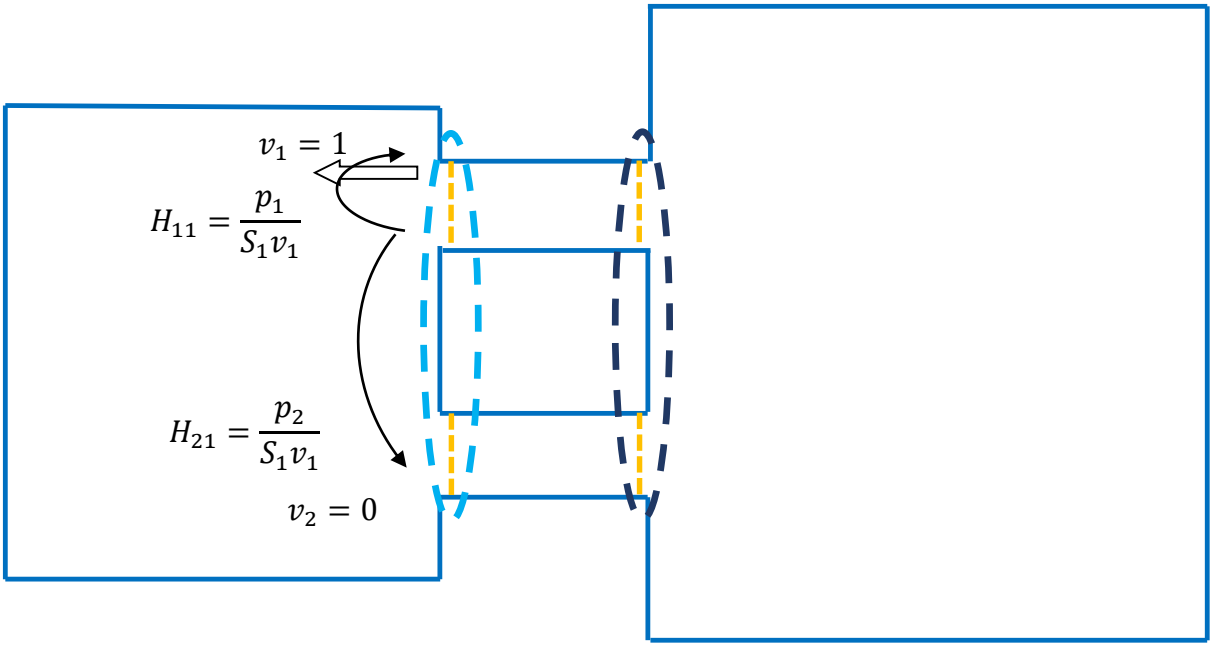

Figure 4.3 Schematic showing transfer functions $H_{11}$and H_{21} between connection points in Room a

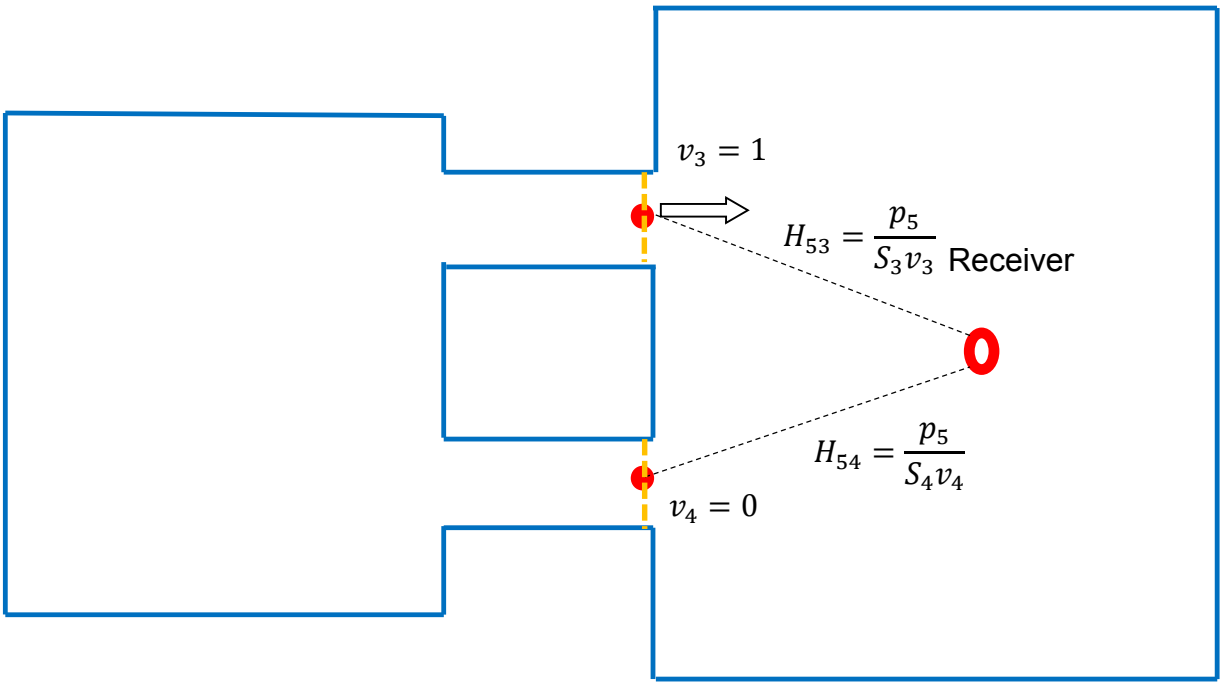

Figure 4.4 Schematic showing receiver Transfer functions

4.1.1.2 Step 2: Determine blocked pressure

The blocked pressure P_{SBi} at each opening was determined by solving the BEM model with all openings closed as shown in Figure 4.5. If the receiver is in the same room with the sources, the blocked sound pressure at the receiver caused by the same-room sources should also be determined.

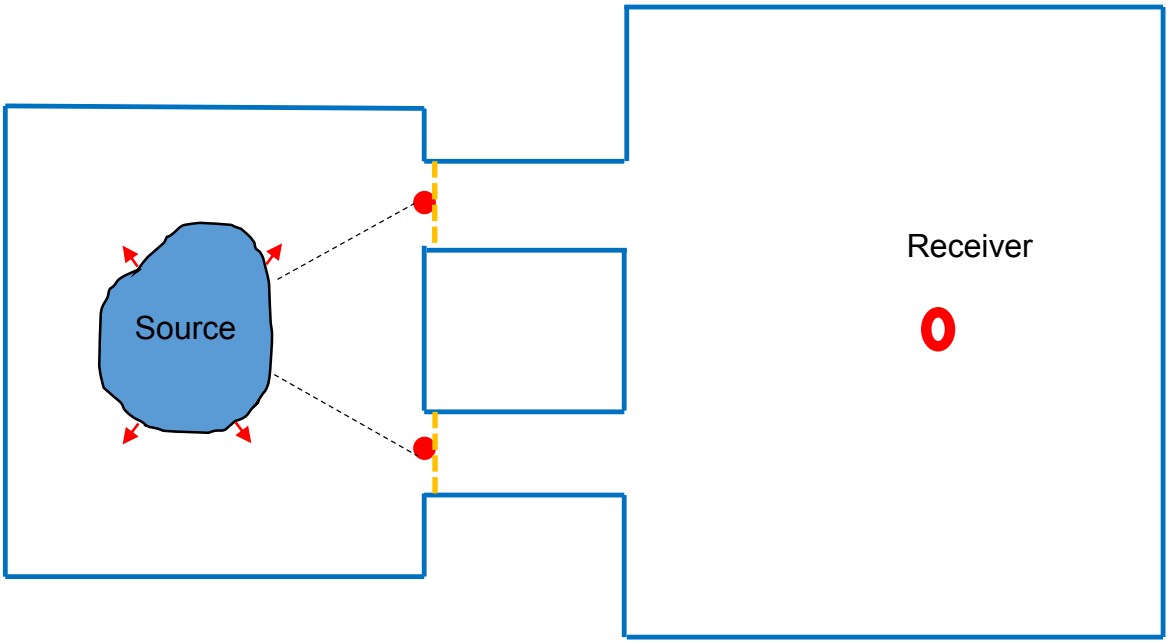

Figure 4.5 Schematic showing blocked pressure in Room a

4.1.1.3 Step 3: Determine transfer matrix of connectors

The transfer matrix of the connection element was calculated analytically. It can also be determined experimentally using either the two-load or two-source methods [28]. The transfer matrix of straight pipes in this case was determined as detailed in Section 3.4.

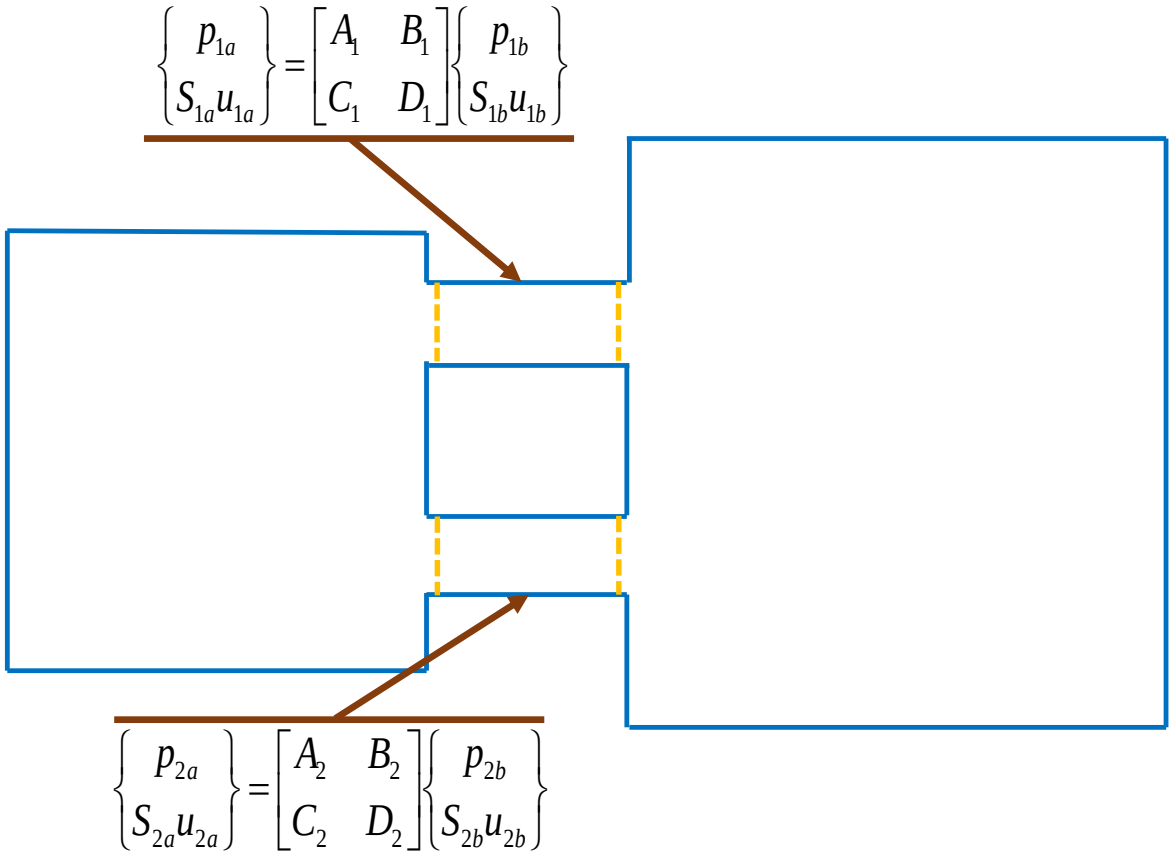

Figure 4.6 Transfer Matrix of Connectors

4.1.1.4 Step 4 Results and Discussion

A comparison of the sound pressure at receiver points using the indirect BEM and the FBS method is plotted in Figure 4.7. The BEM for the complete system and the FBS approach agree well over the full frequency range with only minor differences. These are likely due to the fact that the sound pressure is assumed to be constant over the cross-section of the opening. This assumption will be violated especially at higher frequencies. Nevertheless, the results agree well with the full system model at most frequencies.

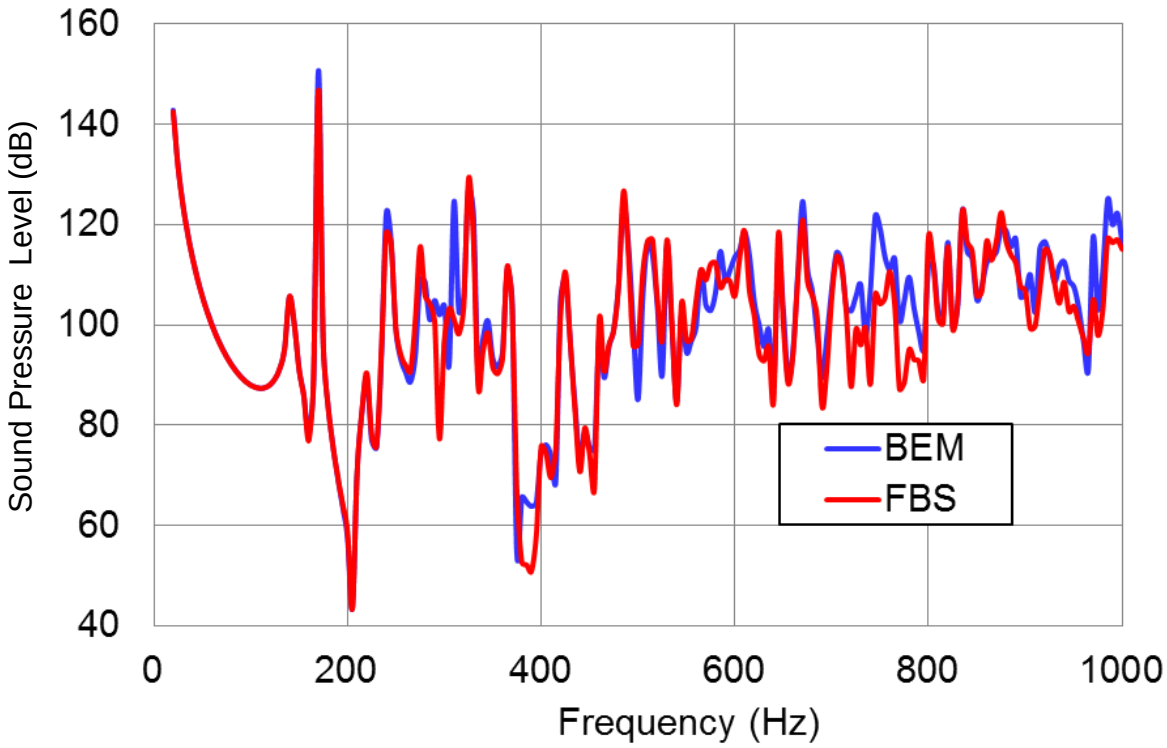

Figure 4.7 Sound pressure level comparison between full model BEM and FBS for system

4.1.2 Two rooms, two pipes, two sets of source

In this section, sources are located in each room. The simulation approach is identical to that in the prior section. There are three monopole sources in Room a and two in Room b. The positions of the sources and the respective source strengths are indicated in Table 4.2. The receiver is set in Room a at the position of (-0.2, 0.2 -0.2) (unit: m). The BEM model is shown in Figure 4.8. There are 5173 nodes and 5174 elements with the element edge length of 0.05 m. The model is valid up to the frequency of 1000 Hz.

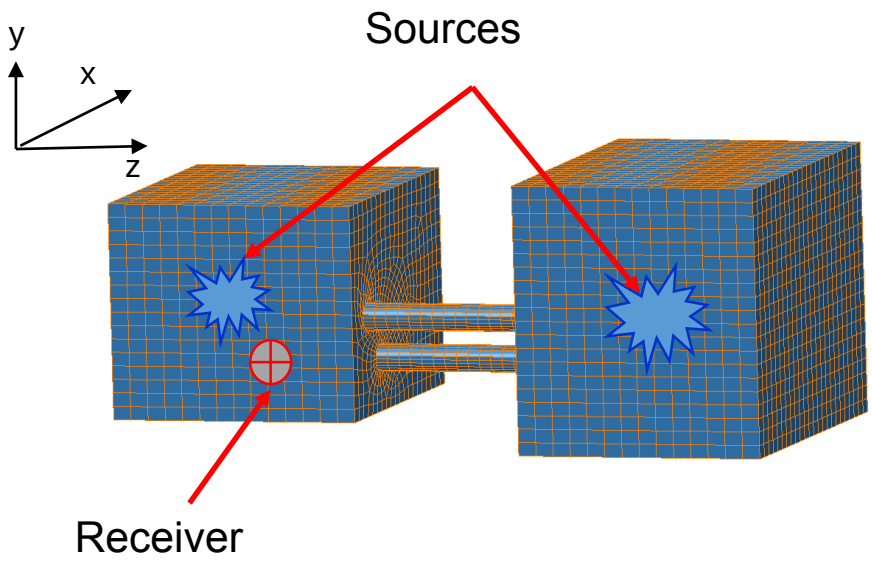

Figure 4.8 Two sources case

Since the receiver and sources are both in Room a, as discussed in the prior section, the blocked sound pressure at the receiver contributed by source a must be determined. All other steps remain the same. Figure 4.9 shows the comparison of FBS and BEM results for the sound pressure level at the receiver. Sound pressure level results compare well. Results are similar to the prior case shown in Figure 4.7. Figure 4.10 shows the contribution from each source and the results indicate that the sources in the second room do not contribute greatly to the sound pressure at the receiver.

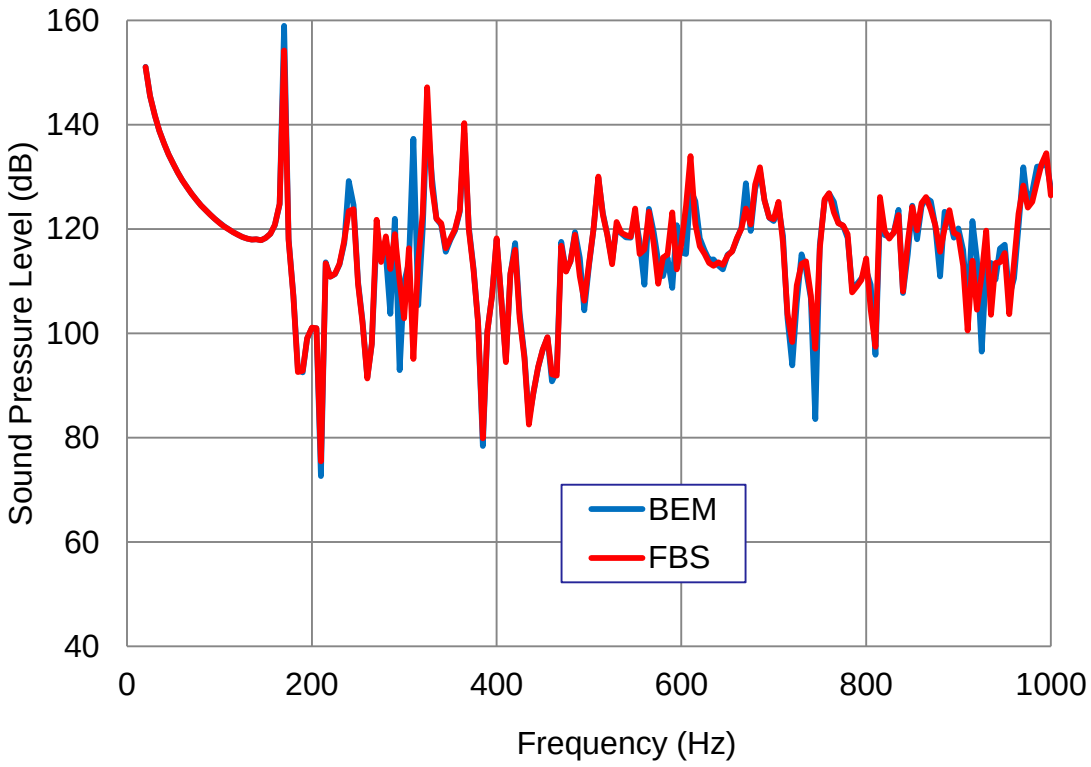

Figure 4.9 Sound pressure level comparison

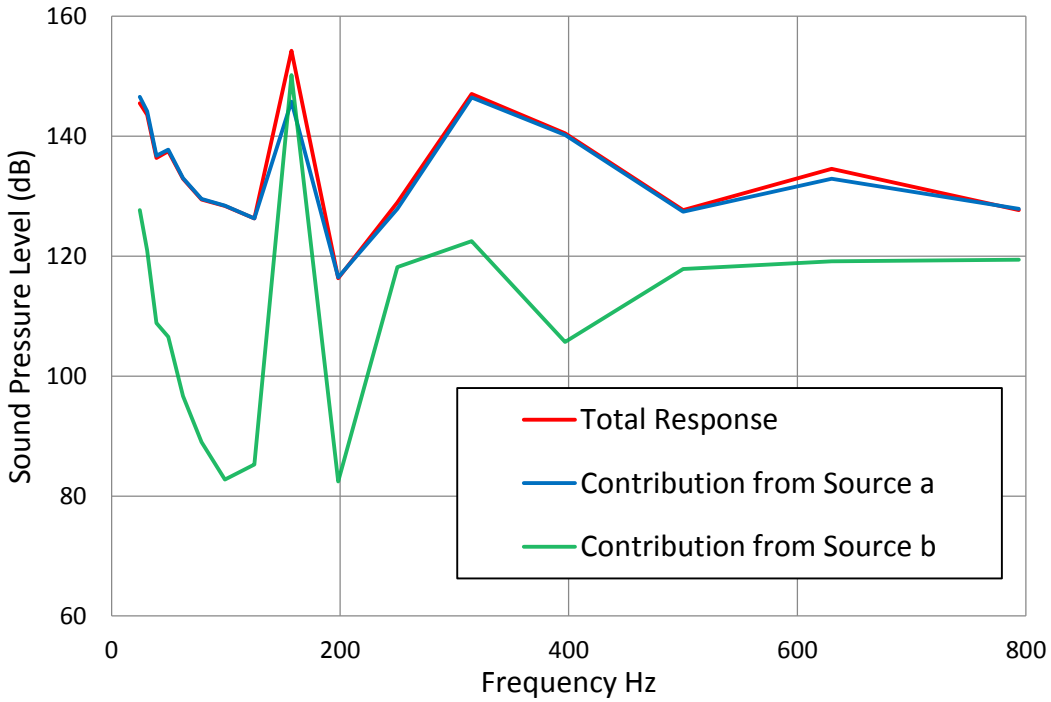

Figure 4.10 Sound pressure level contribution

4.2 Determing the insertion loss

Another validation case is for a single room with two extended pipes radiating noise with no reflections. One-inch thick glass fiber with a flow resistivity of 15000 rayls/m was assumed to be attached to the sides of the room. The complex wave number and characteristic impedance were determined using Equations 6.1 and 6.2 respectively. When the material is attached to a rigid surface, the normal impedance was determined using the expression:

$$Z = -jZ_c \cot(k'L) \tag{4.1}$$

where L is the thickness of the sound absorbing lining. The insertion loss was determined directly using BEM and the sound power predicted by FBS was compared to it. The sound power was determined using the BEM by surrounding the boundary element mesh with a spherical field point mesh and calculating the sound power through the field point mesh.

Figure 4.11 shows a schematic of the setup for determining the insertion loss. Figure 4.12 shows the BEM model with a spherical field point mesh. The whole enclosure is enclosed in the 2 m diameter spherical field point mesh which is comprised of 386 field points. Sound intensity at each field point was calculated using BEM, and the sound power was obtained by Equation 3.31.

The FBS case considers the two openings as two sources. By using Equation 3.18, the sound power was predicted. The FBS and BEM results match well as shown in Figure 4.13.

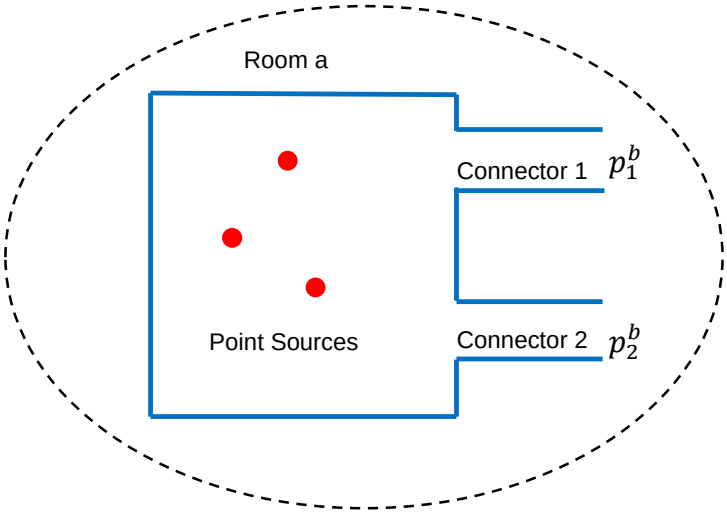

Figure 4.11 Schematic showing one-room sound power insertion loss case.

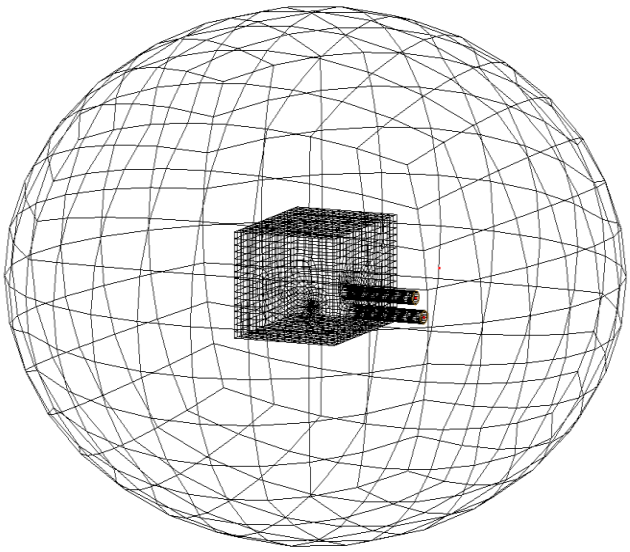

Figure 4.12 BEM model of sound power insertion loss case

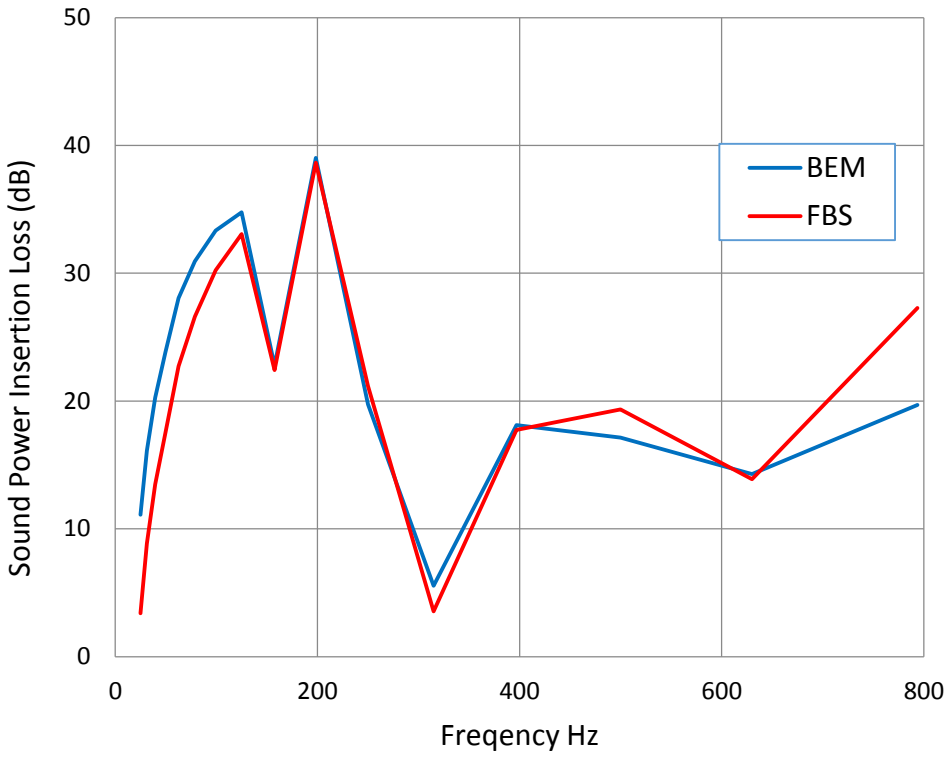

Figure 4.13 Sound power insertion loss comparison

4.3 Results and discussions

The sound pressure at receiver positions and sound power insertion loss determined by the indirect BEM model compares well with the FBS predicted results. This has been validated for a two room case with two connecting ducts between the rooms. In addition, the contribution for a given source to a receiver was determined. The method was also demonstrated for determinging the insertion loss of enclosures.

Chapter 5

EXPERIMENT VALIDATION

In the previous chapter, airborne frequency based substructuring (FBS) including connecting ducts was validated using simulation. In this chapter, an experiment is used to demonstrate the experimental methodology for the FBS approach. The experiment was conducted in the anechoic chamber at the University of Kentucky. The purpose of the experiment was to compare directly measured and FBS calculated receiver sound pressure. Measured transfer functions were used for the FBS approach.

5.1 Enclosure geometry

The partial enclosure used in this chapter is built from 0.75 inch thick particle board. Care was taken to insure that the box was sealed by putty. The two pipes are 2 inch diameter PVC pipe. Figures 5.1 and 5.2 show two views of the enclosure with important dimensions. Two pieces of glass fiber were placed inside the enclosure as shown in Figure 5.3. The flow resistivity of the material used was 15,000 rayls/m, which was measured using ASTM C522 [28]. Figure 5.3 shows a photograph of the inside of the enclosure.

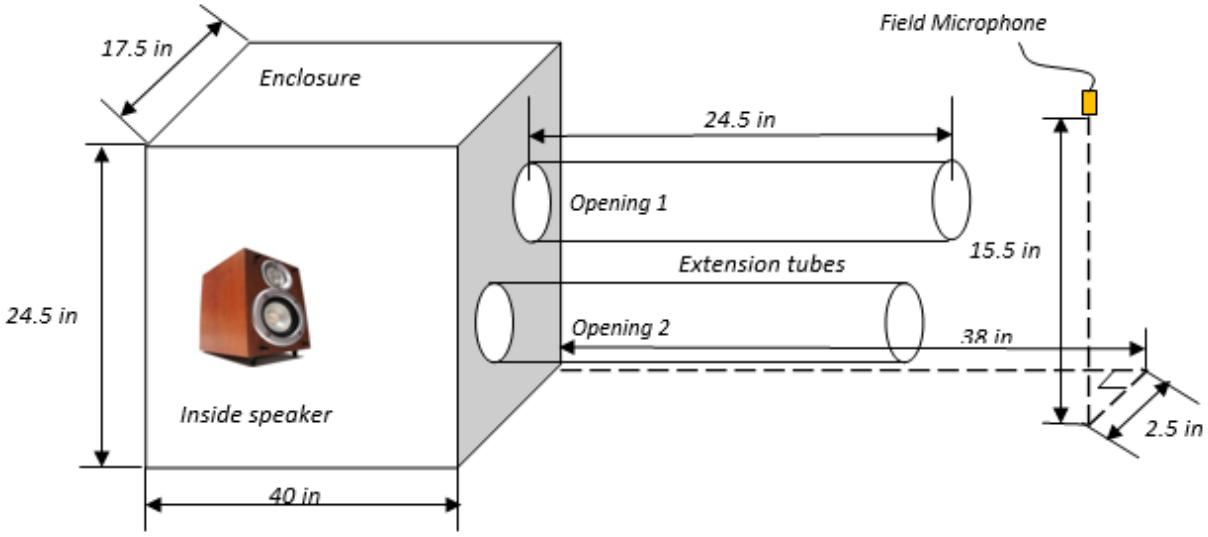

Figure 5.1 Schematic of the enclosure and set up

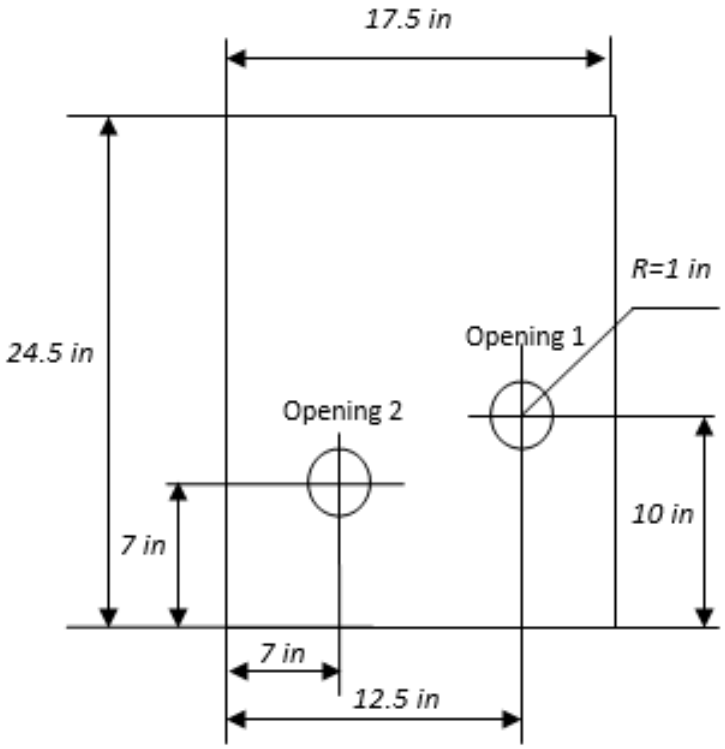

Figure 5.2 Side-view of the enclosure

Figure 5.3 Inside-view of the enclosure

5.2 Equipment

Equipment used in this test includes a Bruel and Kjaer bookshelf loudspeaker, Spectronics impedance tube kit, two PCB microphones, and Microflown PU probe kit. Data was acquired using the LMS SCADAS data acquisition and laptop. The test software used was LMS Test.Lab, and Matlab was used for processing the data. Serial numbers are listed below in Table 5.1. All measurements were made in the hemi-anechoic chamber at the University of Kentucky. The 120 m^3 room is qualified down to 150 Hz.

Table 5.1 Equipment list

Items	*Serial Numbers*
PCB Microphone 1	377B02, SN119297
PCB Microphone 2	377B02, SN119510
Microflown PU Probe Kit	900490
LMS DAQ	SCM01, SN 47122113
Spectronics impedance tube	ACUPRO Version 4

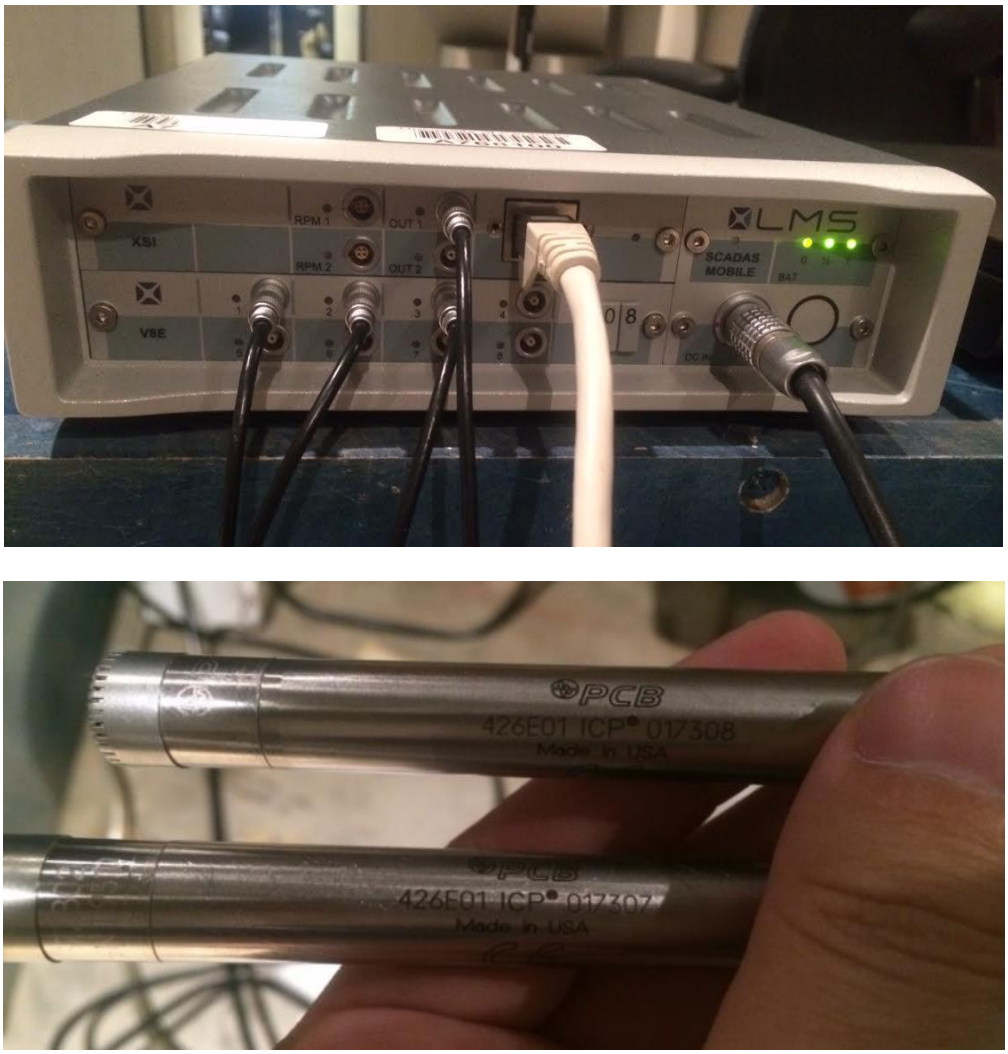

Figure 5.4 LMS 8-channel DAQ (upper) and PCB microphones (lower)

Figure 5.5 PU-probe kit

5.3 Procedure

The procedures used for the experimental study are detailed below. There are five primary steps. These include:

1. Measuring interior transfer functions;

2. Measuring external transfer functions;

3. Measuring blocked or partial sound pressures;

4. Measuring sound pressure in the field;

5. Calculate using the FBS procedure.

5.3.1 Measure interior transfer functions

The first step is to measure the transfer functions between the two duct ports inside the enclosure. Figure 5.6 shows a schematic of the measurement of interior transfer functions H_{11} and H_{21}. In the schematic, the inside loudspeaker is turned off. Opening 1 is open and Opening 2 is blocked with a piece of wood. Opening 1 is connected to an impedance tube. A loudspeaker is located at the end of the impedance tube and is the sound source for the measurement. Two sensors are used in this case. A PU probe is installed in the middle of Opening 1 to measure

the sound pressure and particle velocity at the center of the opening. A microphone is positioned at the center of the blocked opening at position 2 to measure the sound pressure.

When the loudspeaker is turned on, the sound propagates from the loudspeaker into the enclosure through the impedance tube. The particle velocity and sound pressure at Opening 1 is used to determine the transfer function H_{11} . The particle velocity at Opening 1 and the sound pressure at Opening 2 are used to determine the transfer function H_{21}.

The measured transfer functions are expressed as follows.

$$H_{11} = \frac{P_1}{U_1 S_1} \tag{5.1a}$$

$$H_{21} = \frac{P_2}{U_1 S_1} \tag{5.1b}$$

Figures 5.7 and 5.8 are photographs showing the setup for measuring the transfer functions H_{11} and H_{21} . Figure 5.9 shows the loudspeaker attached to the impedance tube.

Following this, the impedance tube and loudspeaker were attached to Opening 2 and Opening 1 is blocked to facilitate measurement of transfer functions H_{12} and H_{22}. The process is identical to this for the other opening.

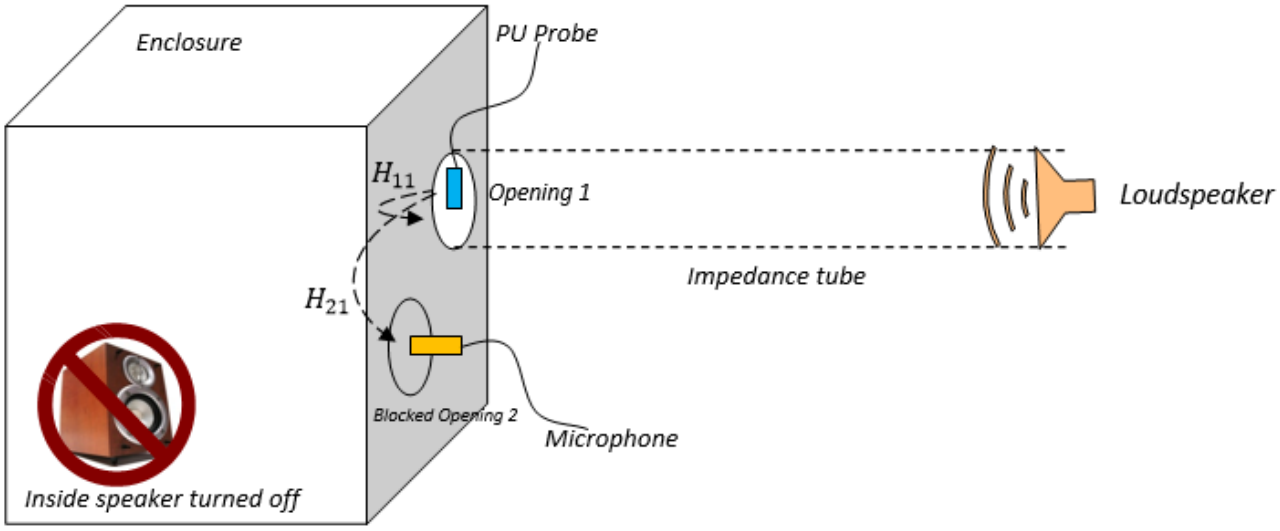

Figure 5.6 Schematic showing process to determine interior transfer functions

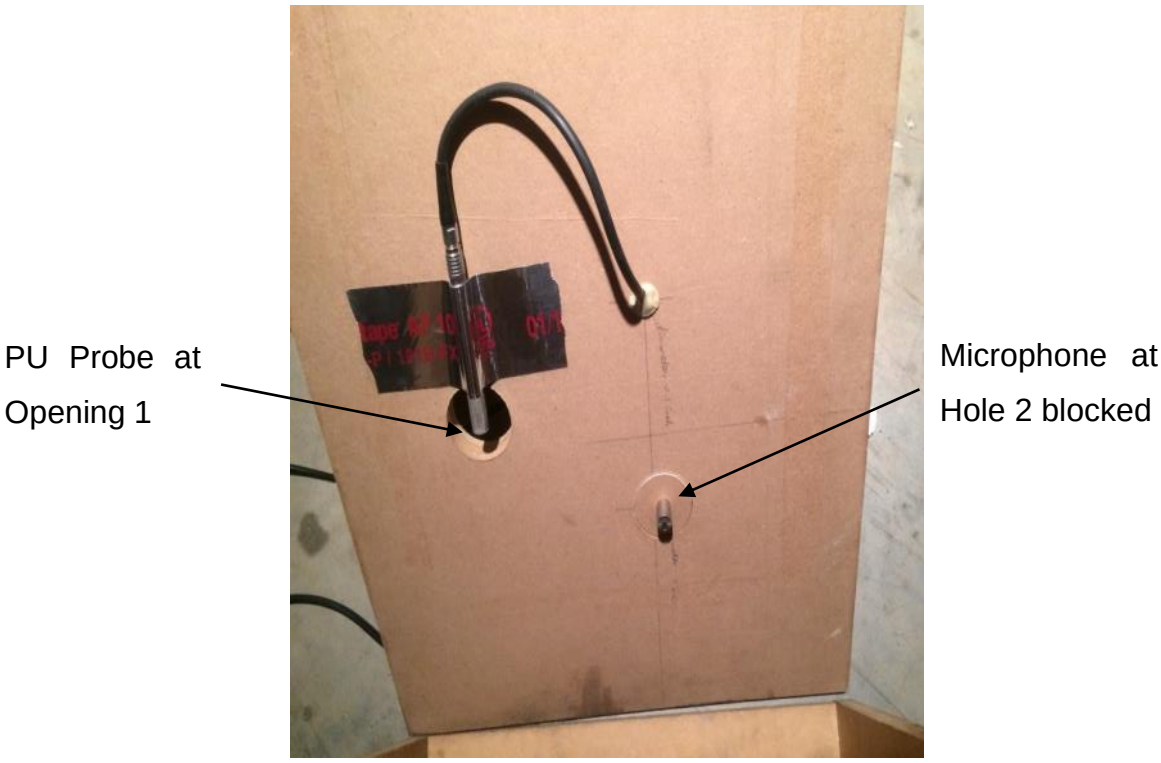

Figure 5.7 Inside-view of the settings for Opening 1 and Hole 2

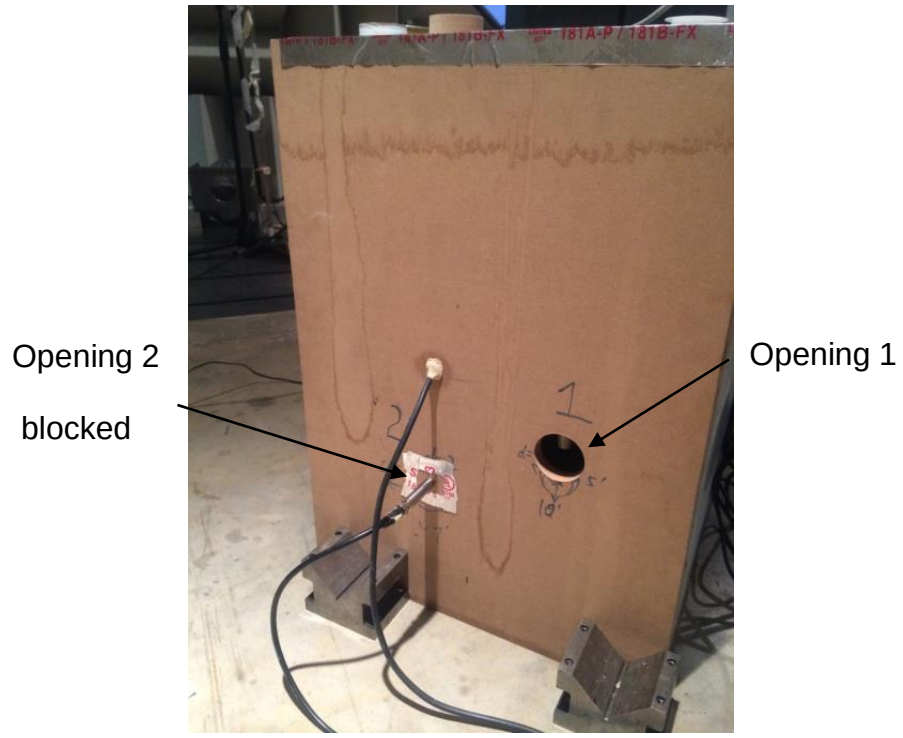

Figure 5.8 Outside-view of settings for Opening 1 and Hole 2

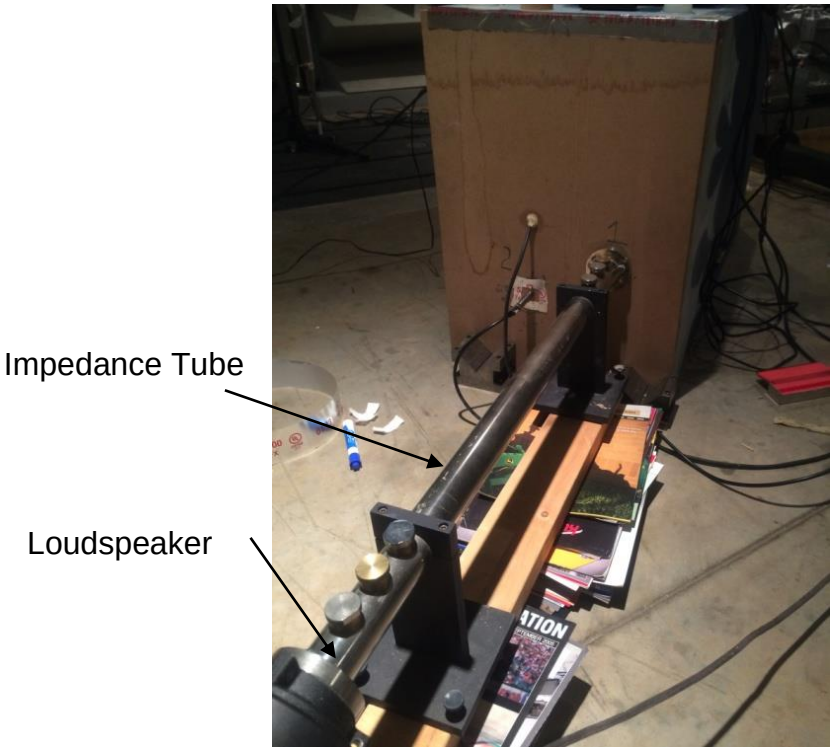

Figure 5.9 Settings for measuring the inside transfer functions

5.3.2 Measure external transfer functions

The second step is to measure the transfer functions between the two openings outside the pipes. Figure 5.10 shows a schematic identifying external transfer functions H_{33}, H_{43} and H_{53} which describe the exterior of the enclosure.

In the schematic, the interior loudspeaker is turned on. Both Openings 1 and 2 inside the enclosure are open and connected to the exterior by PVC pipe. Opening 3 is open but Opening 4 is blocked using a wood board. Three sensors are used. A PU probe is installed in the middle of Opening 3 to measure the sound pressure and particle velocity at the center of the opening. A microphone is positioned at the center of blocked Opening 4. The other microphone is located outside the box and serves as a target response location.

The transfer functions describing the exterior pictured in Figure 5.11 can be determined in an analogous manner. These include H_{33}, H_{43} H_{53} H_{34}, H_{44}, H_{54}. Position 5 corresponds to the receiver.

The transfer function H_{33} is expressed as

$$H_{33} = \frac{P_3}{U_3 S_3} \tag{5.2}$$

Other transfer functions $H_{43}, H_{53}, H_{34}, H_{44}$and H_{54} can be obtained similarly.

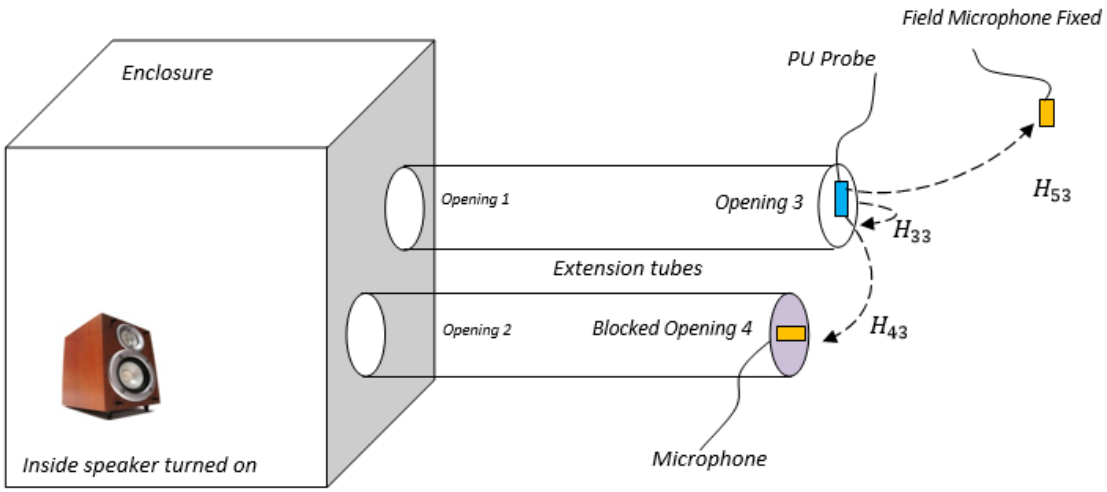

Figure 5.10 Schematic showing the measurement of external transfer functions

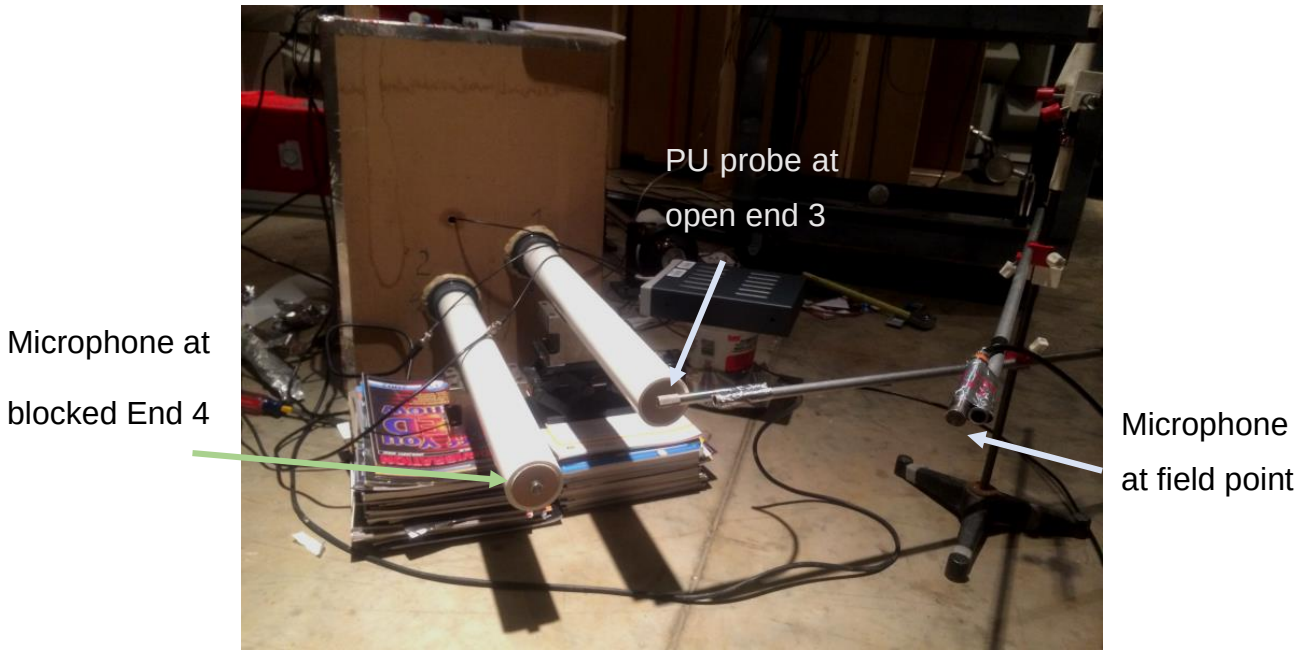

Figure 5.11 Settings for measurement of external transfer functions

5.3.3 Measure blocked or partial sound pressure

This step is to measure the blocked or partial sound pressure at Openings 1 and 2 with both openings blocked. Figure 5.12 shows a schematic of the measurement of blocked or partial sound pressures P_{SB1} and P_{SB2} with the opening blocked. In the schematic, the inside loudspeaker is turned on with signal generated by LMS

Test.Lab. Care was taken to insure that the input signal was the same for all tests. Opening 1 and Opening 2 are blocked with two pieces of wood. A microphone is positioned at the center of each opening. The phase of the sound pressure is determined using the loudspeaker signal as a reference. Figure 5.13 shows a photograph of the measurement test setup.

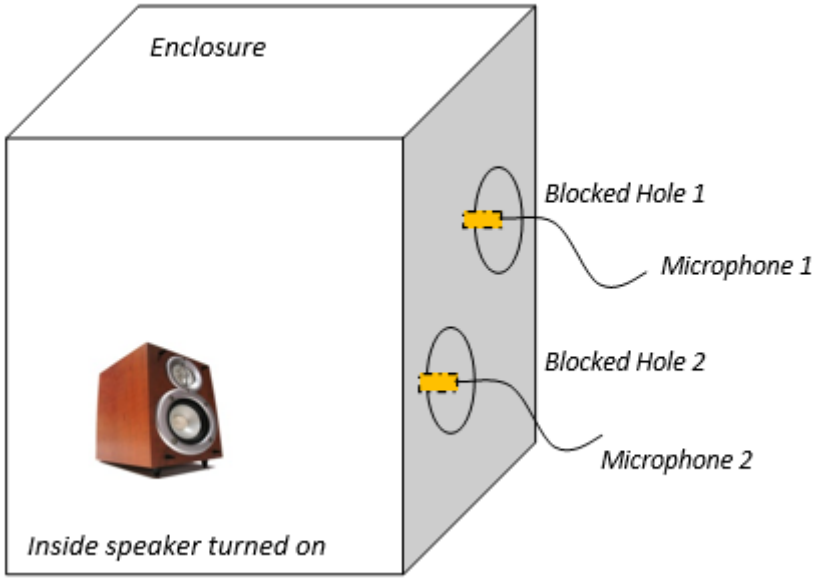

Figure 5.12 Schematic of the measurement of blocked or partial sound pressure

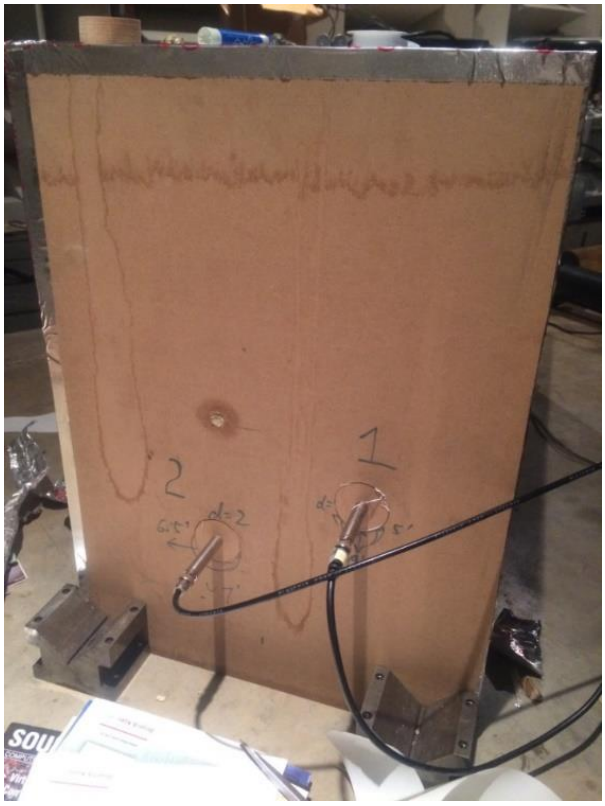

Figure 5.13 Photograph showing setup for measurement of blocked or partial sound pressures

5.3.4 Measure sound pressure in the field

The actual sound pressure at the receiver point was then measured and used to compare to the FBS determined sound pressure. Figure 5.14 shows a schematic of the relative position of the receiver point with respect to the two outlet pipes. Care was taken to insure that the loudspeaker level remained the same throughout the testing.

The sound power from the two openings was measured using the same setup. A measurement surface enclosing the two openings was created using string and a frame. The sound intensity was scanned for each surface using ISO-9614. Figure 5.15 shows the measurement setup.

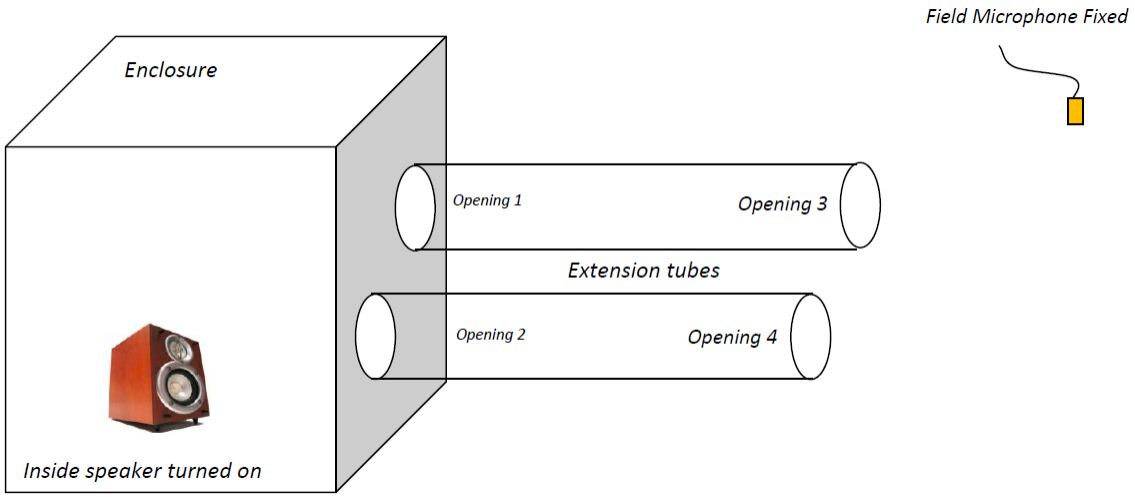

Figure 5.14 Schematic of sound pressure measurement in working condition

Figure 5.15 Settings for sound pressure measurement in working condition

5.3.5 Calculate using the FBS Procedure

All the data collected in the four steps was imported to MATLAB for FBS calculation. The voltage data from the PU-probe was converted to Pa and m/s using the calibration curve provided by Microflown Inc. The transfer matrix of the connecting

pipes was determined using Equation 3.19. The equations used for the calculations are detailed in Chapter 3.

5.4 Results and Discussion

5.4.1 Sound pressure prediction

Sound pressure at the receiver point was measured directly and calculated using the FBS method. Results are compared in Figure 5.16. In this case, the pipe's diameter is 2 inches, which means the plane wave cut-off frequency is around 4000 Hz [26]. The blue curve is the direct measurement and the red curve shows the FBS prediction. Sound pressure levels are comparable but there are obvious differences. Differences may be due to the highly reverberant nature of the enclosure since very little sound absorption was added to the interior. Additionally, the measurement procedure for determing the volume velocity using the P-U probe and additional measurement protocols should be reviewed. At this juncture, results are inconclusive. It is recommended that measurement research continue to prove out the method.

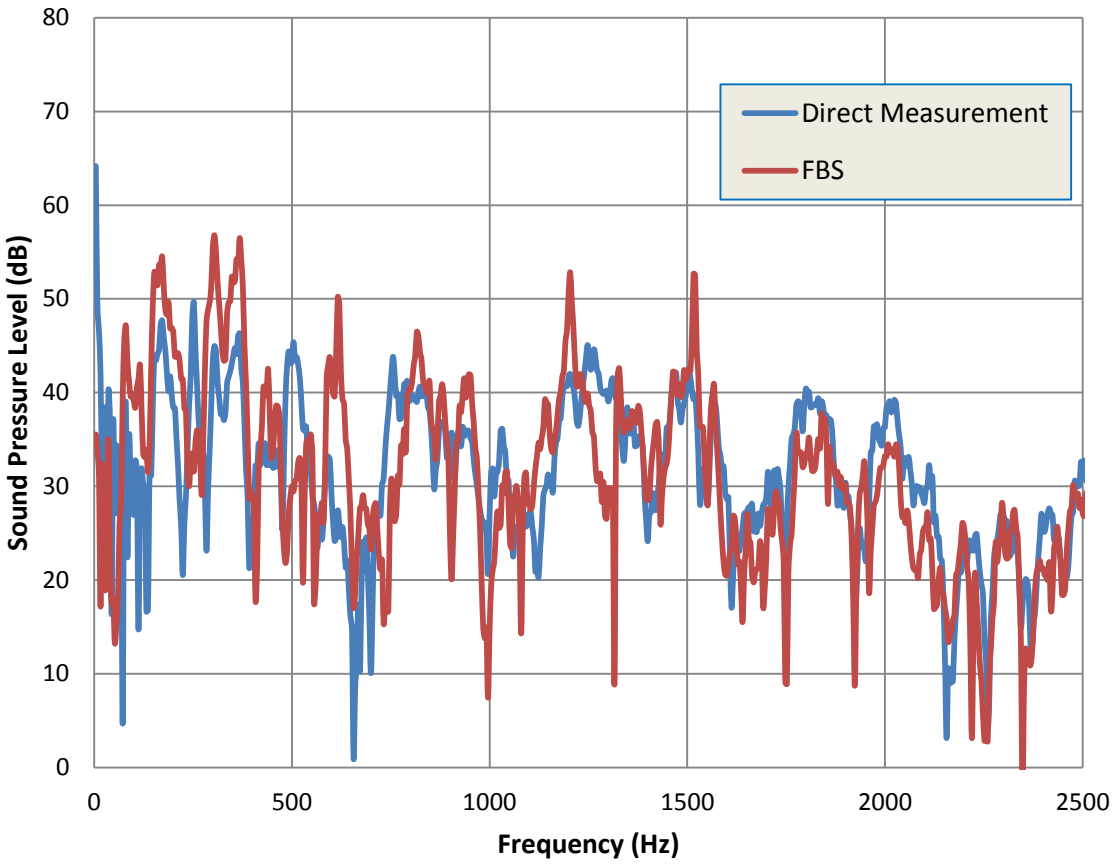

Figure 5.16 Results of Receiver Sound Pressure Prediction

5.5 Summary

In this chapter, the FBS method was applied experimentally to a partial enclosure. Sound pressure predictions are on the same order of magnitude as those measured but there are some noticeable differences. It is recommended that the measurements in this chapter be repeated with a less reverberant enclosure.

Chapter 6

APPLICATION OF AIRBORNE FREQUENCY BASED SUBSTRUCTURING TO REDUCE ENCLOSURE NOISE

Frequency based substructuring (FBS) is a procedure in which structural or acoustic subsystems and connections are simulated by transfer functions. FBS is routinely applied to determine the structural response. It is advantageous for a number of reasons. First, subsystem and connection transfer functions can be determined numerically or experimentally. As such, the method is a convenient way to combine numerical and experimental component models into an overall system model. Additionally, connection and some component modifications may be considered without the need to reanalyze the complete system. Additional benefits include the ability to identify sources based on the measured transfer functions and operational data and to determine contributions. FBS is sometimes referred to as transfer path analysis (TPA).

In previous chapters, the method for airborne subsystems and connections was detailed. In this case, airborne subsystems refer to rooms or enclosure volumes and connections to ducts running between the subsystems. The procedure was validated for a two room case and was also used to determine the insertion loss for a partial enclosure.

This chapter will demonstrate the applicability of the approach for path contribution analysis, modifications to connecting ducts, and adding lumped impedance attenuation devices (Helmholtz resonators or quarter wave tubes) to a subsystem.

6.1 Path contribution analysis

In Equation 3.17b, the individual terms on the right hand side represent the contributions from connections a and b and the sources s to the sound pressure in either Room a or b. Once the contributions are well understood for a particular problem, treatments can be considered and simulated to evaluate their effectiveness.

The two-room with two-connection case is used as an example. The source is assumed to be present in Room a and the receiver in Room b. To determine the contribution from each opening to the passive room, a contribution analysis was carried out using airborne FBS. For structureborne analyses, contribution analysis is commonly used to assess the contributions from the forces at respective mounting points. For airborne paths, the contribution from each opening was determined. LMS Virtual.Lab was used for all simulations.

The BEM model is shown in Figure 6.1. The dimensions of the room are indicated in Table 4.1. Three unit monopole sources are located in Room a. A receiving point or field point was positioned in Room b. There are 5173 nodes and 5174 elements in the model with an element edge length of 0.05 m. The model is valid up to 1000 Hz. Three unit amplitude monopoles were positioned in Room a having the same phase. The length and the diameter of the connecting pipes were 0.5 m and 0.1 m respectively.

The transfer functions were calculated using the method discussed in the previous section. Two BEM runs were performed for each room to determine the required transfer functions. The blocked pressure (P_1^a and P_2^a) at each opening in Room a was determined by solving with the source active and all openings closed. The transfer matrix for the connecting ducts was determined using transfer matrix theory.

After the FBS analysis, results were compared with BEM simulation of the entire system using the mesh shown in Fig. 6.1. The total response and the contribution from each duct are shown in Figure 6.2. For the receiver point selected,

Connection 1 contributes more to the sound pressure level at the receiver than Connection 2. The results demonstrate how FBS can be used to identify the dominant energy paths.

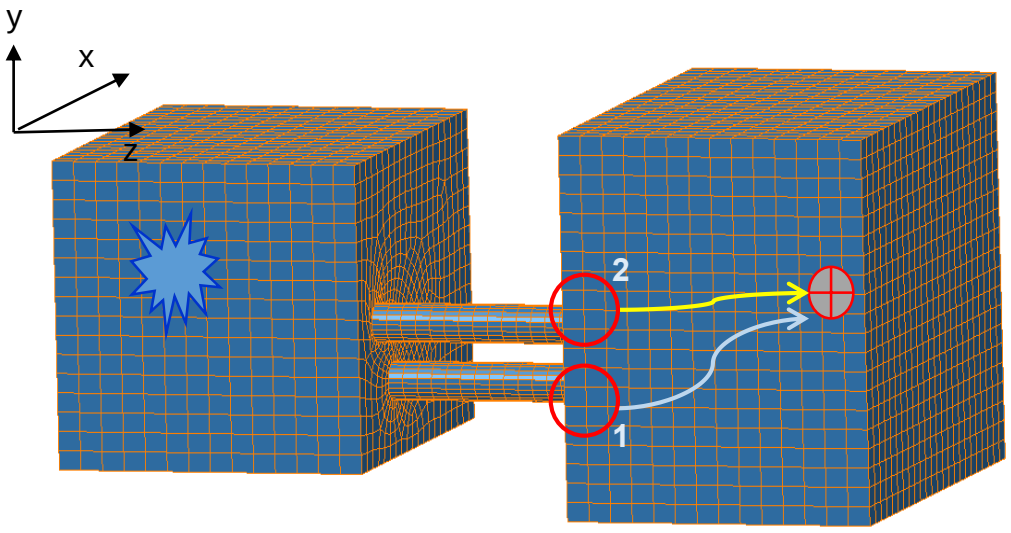

Figure 6.1 BEM model of path contribution analysis

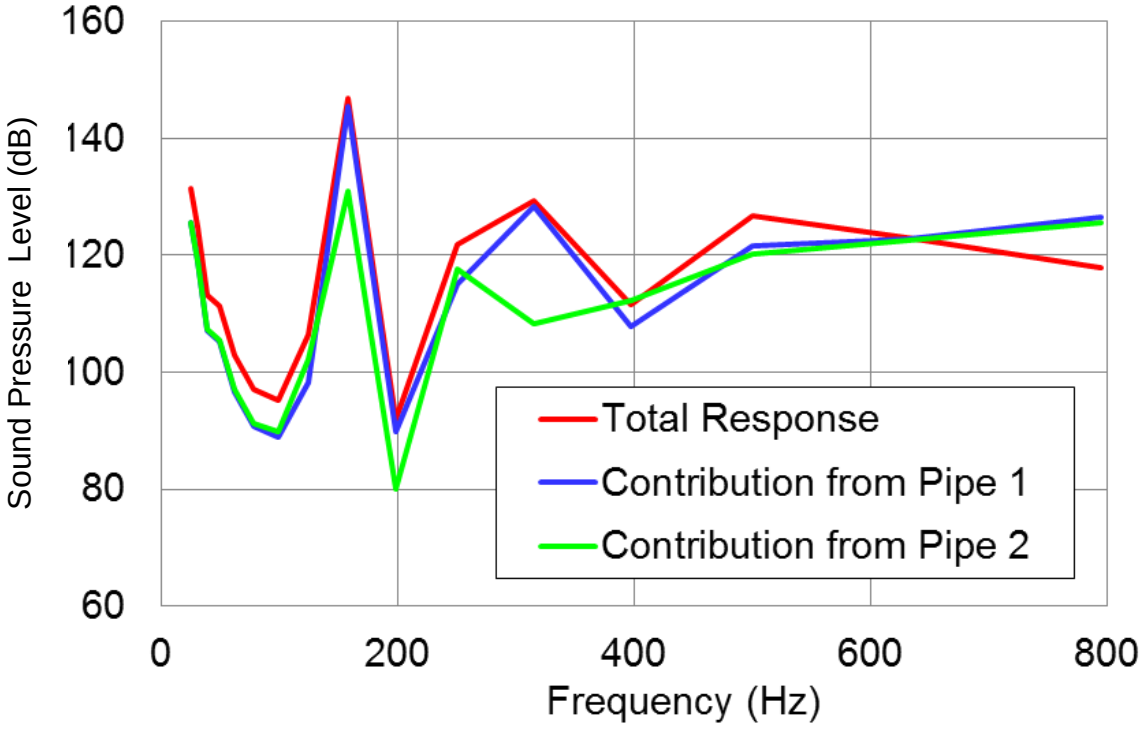

Figure 6.2 Path contribution analysis results

6.2 Adding expantion chambers

Connections between the two rooms are represented as a transfer matrix. In this example, an expansion chamber is positioned in the connecting duct. A schematic of the connection with added muffler is shown in Figure 6.3 and the BEM model is shown in Figure 6.4. The transfer matrix of the muffler is calculated by multiplying three transfer matrices of straight pipes with lengths of *0.2 m, 0.05 m,* and *0.25 m* using transfer matrix theory (See Section 3.4). Sound pressure level comparisons are shown in Figure 6.5 with good agreement.

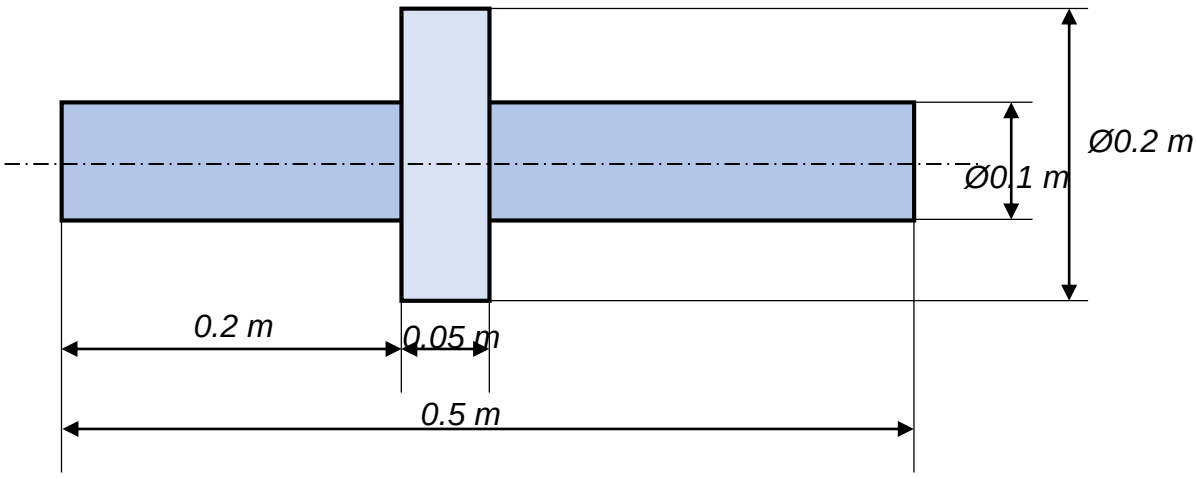

Figure 6.3 Cross-section of a muffler

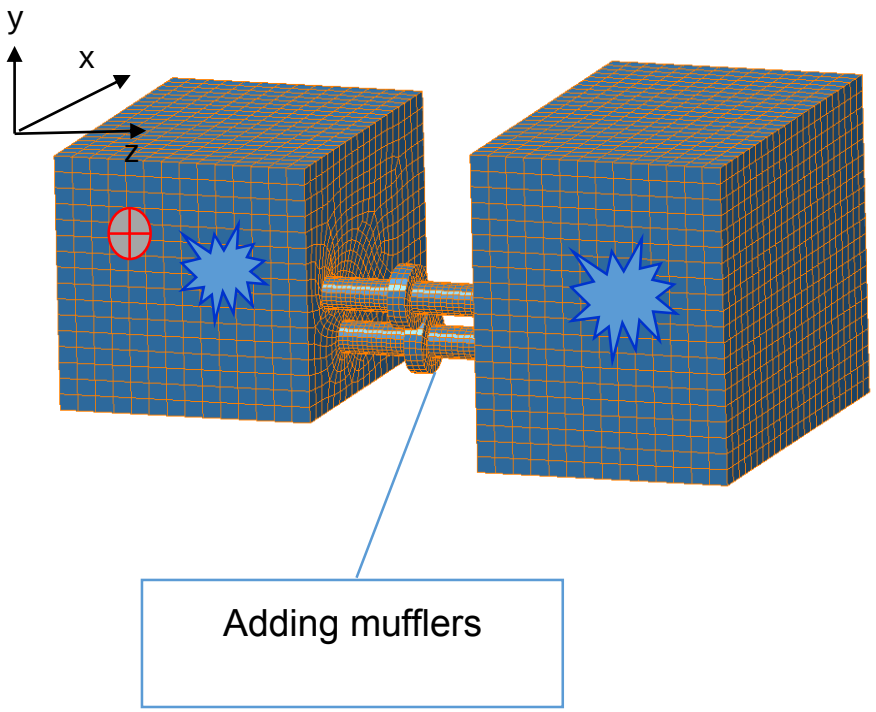

Figure 6.4 Adding two mufflers

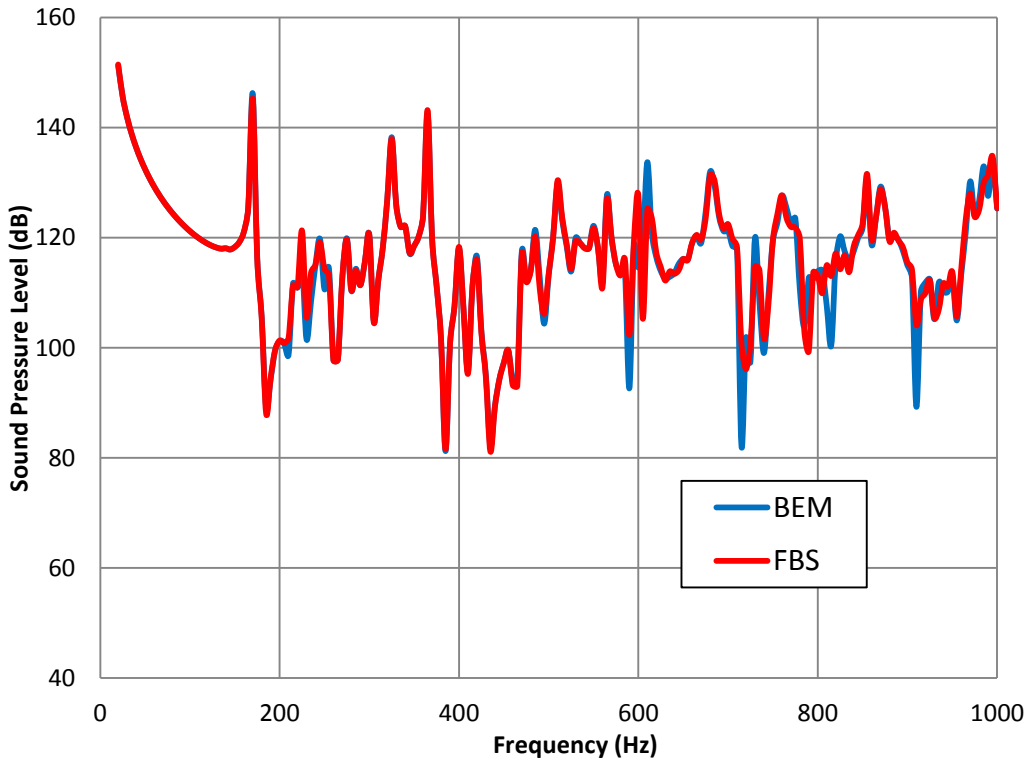

Figure 6.5 Sound pressure level comparison

6.3 Adding absorption filling

To improve the attenuation performance at the receiver points, treating the connecting pipes with a sound absorptive fill was considered. Glass fiber with a flow resistivity of 15,000 rayls/m was assumed. The complex wave number and characteristic impedance were determined using Mechel's [29] model. The complex wave number k' can be expressed as:

$$k' = \beta - j\alpha \tag{6.1}$$

where β is called the phase constant or propagation constant, while, α is known as the attenuation constant. Usually k' is measured directly for a given material. The characteristic impedance of the porous material is Z_c, which is equal to the sound pressure divided by particle velocity expressed as:

$$Z_c = \frac{p(x)}{u(x)} \tag{6.2}$$

Given the complex wave number k' and characteristic impedance Z_c for an acoustic material, the transfer matrix of the filled duct can be written as:

$$\begin{Bmatrix} p_1 \\ S_1 u_1 \end{Bmatrix} = \begin{bmatrix} \cos k'L & \frac{jZ_c}{S_2}\sin k'L \\ \frac{jS_1}{Z_c}\sin k'L & \frac{S_1}{S_2}\cos k'L \end{bmatrix} \begin{Bmatrix} p_2 \\ S_2 u_2 \end{Bmatrix} \tag{6.3}$$

where L is the length of the fill in the duct.

The BEM model used for validation is shown in Figure 6.6. The sound pressure at the receiver point with and without glass fiber treatment is shown in Figure 6.7.

With the absorption material added, the sound pressure level at the receiver decreased by 40 to 70 dB over the frequency range. As anticipated, filling the ducts with glass fiber greatly improves the acoustic attenuation in the ducts.

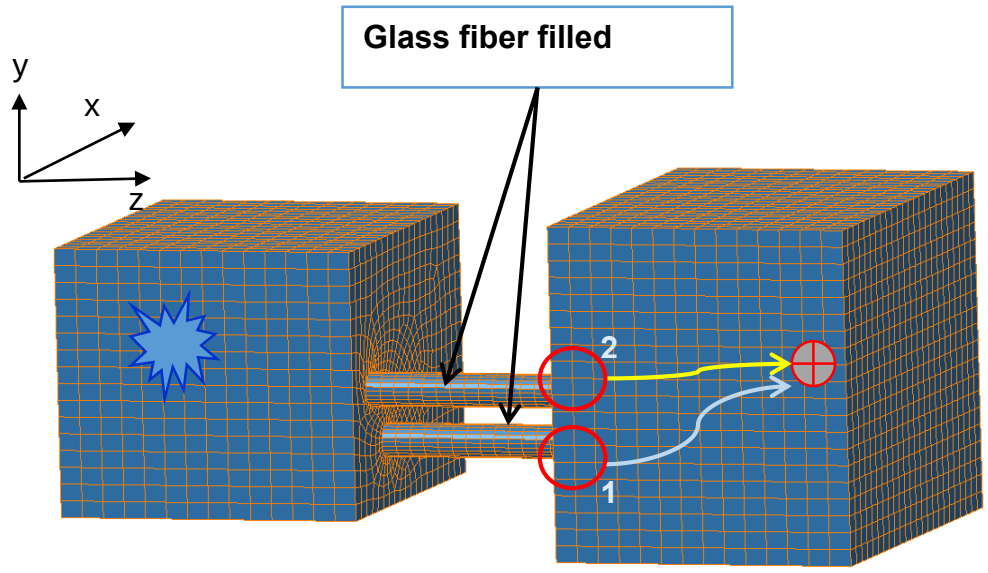

Figure 6.6 BEM model showing where glass fiber is filled

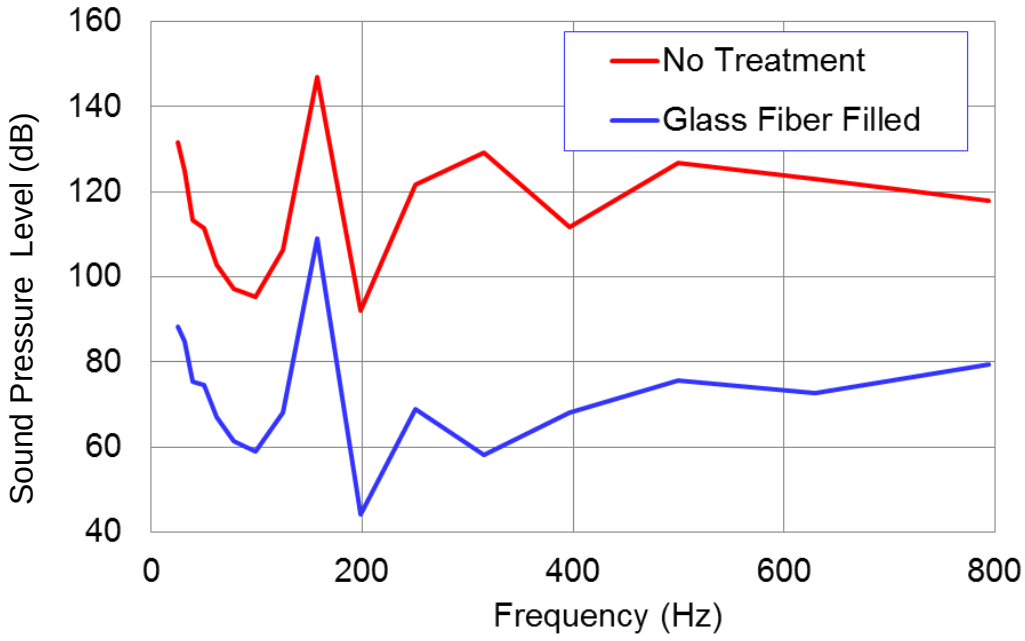

Figure 6.7 Glass fiber effect using FBS

Another treatment considered was one pipe filled with glass fiber and the other with muffler added, as shown in Figure 6.8. Figure 6.9 shows the difference in sound pressure at the receiver when adding the muffler in one duct and glass fiber in the other. It is apparent that the response through the muffler path is dominant and that the muffler is especially effective at 315 Hz. Figure 6.10 shows the sound pressure insertion loss by adding muffler and glass fiber.

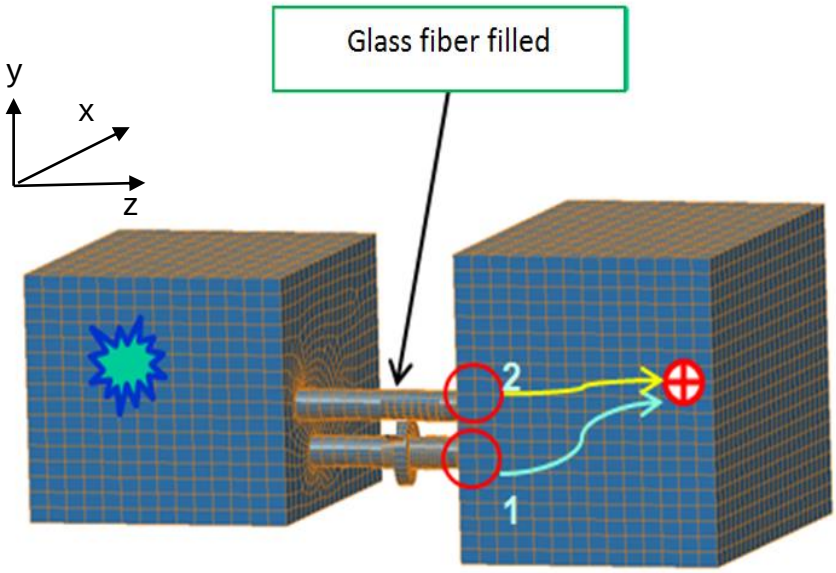

Figure 6.8 One muffler and one pipe with glass fiber

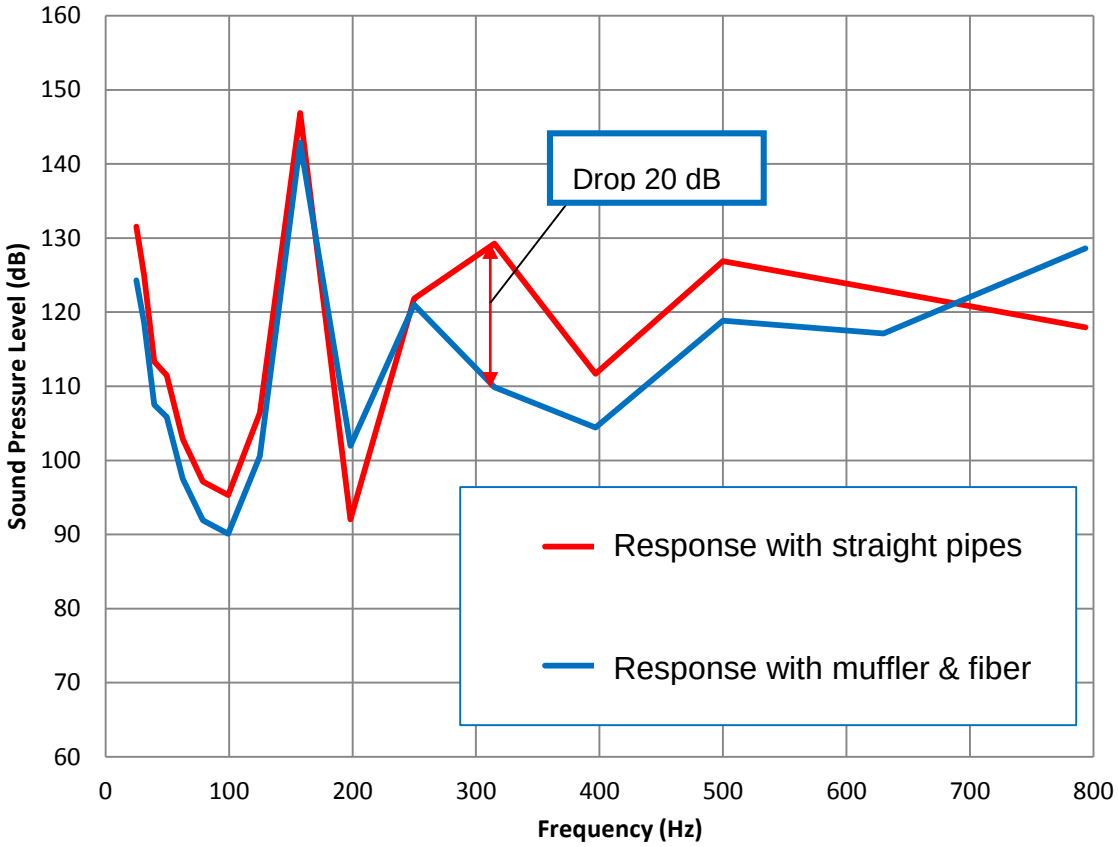

Figure 6.9 Effect of adding muffler and glass fiber

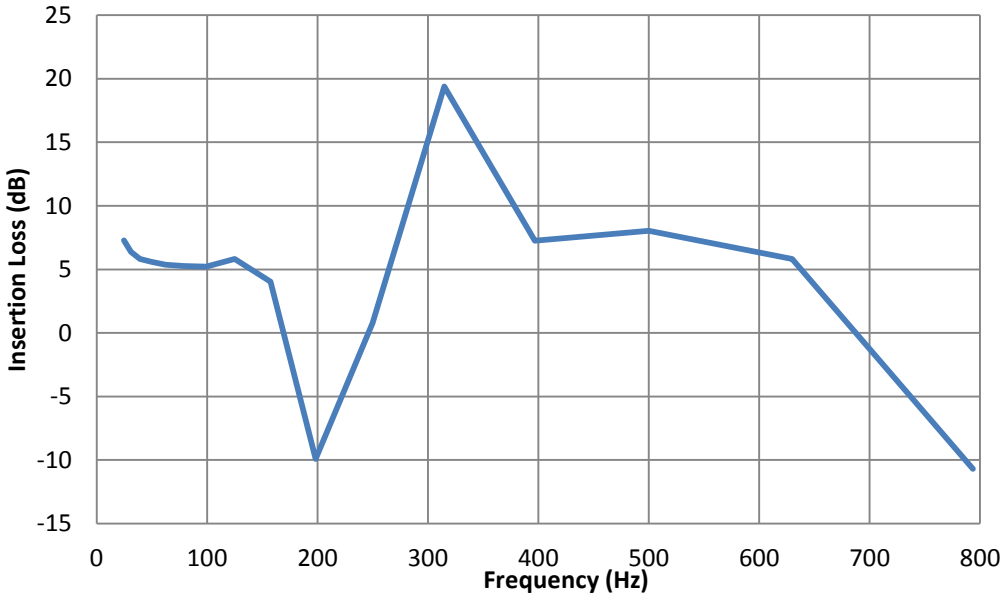

Figure 6.10 Insertion loss of adding muffler and glass fiber

6.4 Adding Helmholtz resonators

Consider adding two side branches to the middle of the two straight pipes. Commonly used side branches include Helmholtz resonators and quarter wave tubes. A Helmholtz resonator consists of a neck connected to a comparatively large volume. The added Helmholtz resonators were tuned to approximately 325 Hz to each duct. The adjusted neck length neck diameter, and cavity volume were 8.8 cm, 10 cm and 0.0025 m^3 respectively. The sound pressure level at the field point in the two-room case with straight pipes and Helmholtz resonators is shown in Figurer 6.11. The Helmholtz resonator is effective at the targeted frequency of 325 Hz but is ineffective at other frequencies.

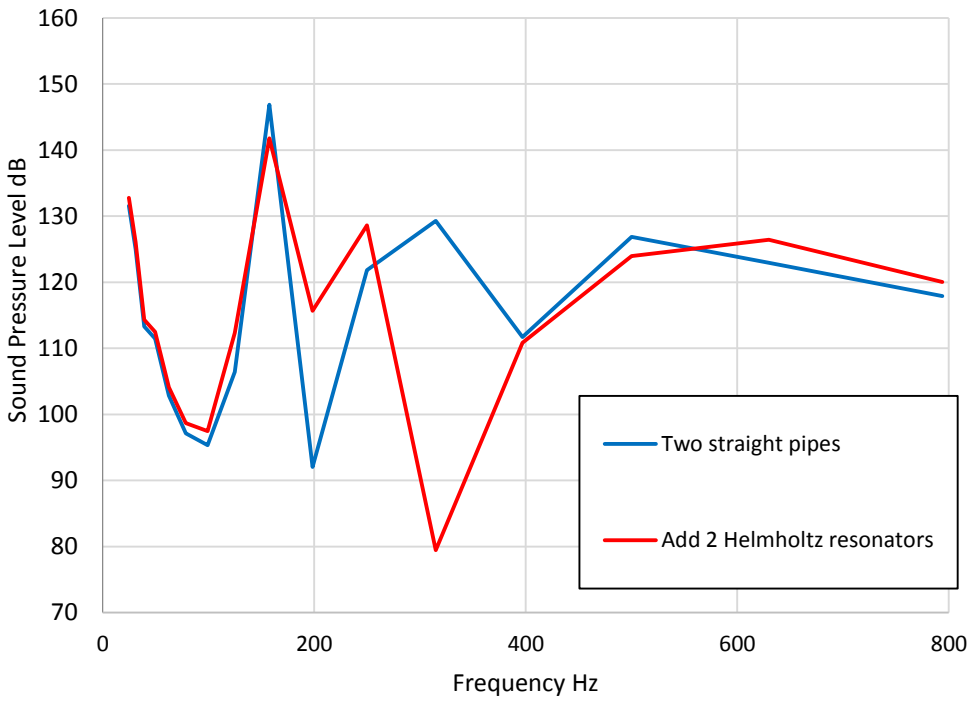

Figure 6.11 Sound pressure level without and with Helmholtz resonators added

6.5 Lumped impedance treatments to subsystems

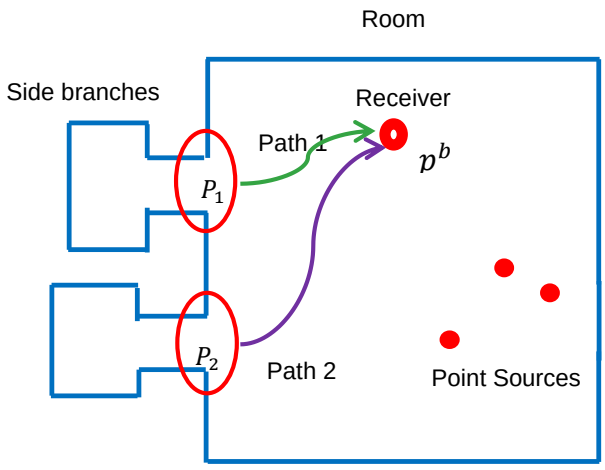

Figure 6.12 Schematic showing test case with side branches

The FBS approach is also valuable for investigating the effectiveness of lumped impedance treatments for the subsystems. The equations for the lumped elements are detailed in Appendix B. Here a single-room case with side branches is introduced in Figure 6.12. Each side branch can be considered as a lumped impedance. For each lumped impedance, the sound pressure (P_i) and volume velocity ($S_i U_i$) are related via the impedance (Z_i) so that:

$$P_i = Z_i S_i U_i \, , i = 1,2 \tag{6.4}$$

This can be expressed as an impedance matrix where the sound pressures and particle velocities are related to one another via

$$\begin{Bmatrix} P_1 \\ P_2 \end{Bmatrix} = \begin{bmatrix} Z_1 & 0 \\ 0 & Z_2 \end{bmatrix} \begin{Bmatrix} S_1 U_1 \\ S_2 U_2 \end{Bmatrix} . \tag{6.5}$$

The respective particle velocities and sound pressures can also be related to one another via

$$\begin{Bmatrix} P_1 \\ P_2 \end{Bmatrix} = \begin{bmatrix} H_{11} & H_{12} \\ H_{21} & H_{22} \end{bmatrix} \begin{Bmatrix} S_1 U_1 \\ S_2 U_2 \end{Bmatrix} + \begin{Bmatrix} P_1^a \\ P_2^a \end{Bmatrix} \tag{6.6}$$

where H_{ij} are transfer functions relating the sound pressure and volume velocity at the lumped impedance positions and P_1^a and P_2^a are the blocked sound

pressures at the lumped impedance positions when the openings are blocked and the internal source is active. Combining Equations 6.5 and 6.6, the volume velocities can be determined via

$$\begin{Bmatrix} S_1U_1 \\ S_2U_2 \end{Bmatrix} = \left(\begin{bmatrix} Z_1 & 0 \\ 0 & Z_2 \end{bmatrix} - \begin{bmatrix} H_{11} & H_{12} \\ H_{21} & H_{22} \end{bmatrix} \right)^{-1} \begin{Bmatrix} P_1^a \\ P_2^a \end{Bmatrix} . \quad (6.7)$$

Once the volume velocities and the transfer functions from the side branch inlets to the target receivers (H_{Ti}) are determined, the sound pressure at a receiver (P_T) can be expressed as:

$$P_T = H_{T1}S_1U_1 + H_{T2}S_2U_2 + P_T^a \quad (6.8)$$

where P_T^a is the blocked sound pressure at the target.

A single room with three point monopole sources was considered. Two resonators were attached to the wall as a treatment with an aim to reduce the sound pressure at a receiver position in the room. A schematic of the case considered is shown in Figure 6.12 and a BEM model of the room plus one and two resonators are shown in Figure 6.13 and 6.14 respectively.

The room had dimensions of $4.5\ \mathrm{m} \times 4.5\ \mathrm{m} \times 4.5\ \mathrm{m}$. There were two Helmholtz resonators (R1 and R2) attached to the wall as shown in Figures 6.15. The neck diameter of the Helmholtz resonators is $0.65\ \mathrm{m}$. The neck length was 48.8 cm for both resonators and the attached volume was $1\ \mathrm{m}^3$ and $0.5\ \mathrm{m}^3$ for R1 and R2 respectively. Three unit point sources were positioned in the machine room at coordinates of (2.0, 3.0, 1.5), (2.5, 1.8, 3.0) and (1.0, 2.5, 1.5) (unit: m) and were in phase with one another. Three panels of 2.5 cm thick sound absorbing material ($2.4\ \mathrm{m} \times 3.3\ \mathrm{m}$) were centered on three walls. The sound absorption coefficient

was determined using Mechel's equation for fiber assuming a flow resistivity of $15{,}000$ rayls/m. The receiver was positioned at (1.2, 0.2, 1.5) (unit: m).

The finite element analysis was performed in LMS Virtual.Lab. The element edge edge length was 0.3 m, so analyses should be valid up to 180 Hz.

For the first case, a BEM model of a single room without resonators was built with the point sources and receivers set as above. This model was also used to determine the transfer functions (H_{ij} and H_{Ti}) in Equations (13) and (14). After which, a BEM model of a single room with resonators R1 and R2 was constructed (Figure 6.17). The sound pressures at receivers were obtained by both BEM calculation and FBS prediction. The resonant frequencies of the Helmholtz resonators R1 and R2 are 37.5 Hz and 54.5 Hz respectively. The impedance at the resonator inlets were calculated numerically in order to accurately include inertial effects.

In the first baseline case, a BEM model of a single room without resonators was built. With the point sources and receivers set as above, the sound pressures at receivers were obtained by BEM calculation as the baseline.

In the second case, a BEM model of a single room with resonator R1 was built (Figure 6.13). With the same point sources and receivers as in the baseline, the sound pressures at receivers were obtained by both BEM calculation and FBS prediction. The tuned frequency of the Helmholtz resonator R1 is 37.5 Hz.

In the third case, there was an additional resonator R2 added to the model (Figure 6.14). Similarly the sound pressure at receivers were obtained using both BEM and FBS. The tuned frequency of the Helmholtz resonator R2 is 54.5 Hz.

In the fourth case, two Helmholtz resonators in Case Three were replaced with two quarter wave length resonators which were tuned at the same frequencies as the Helmholtz resonators.

In each case, the impedances at the resonator inlets were calculated using the equations in Appendix B. The transfer functions and blocked sound pressure were obtained using BEM simulation. The data was imported into MATLAB and the responses were determined using the FBS method.

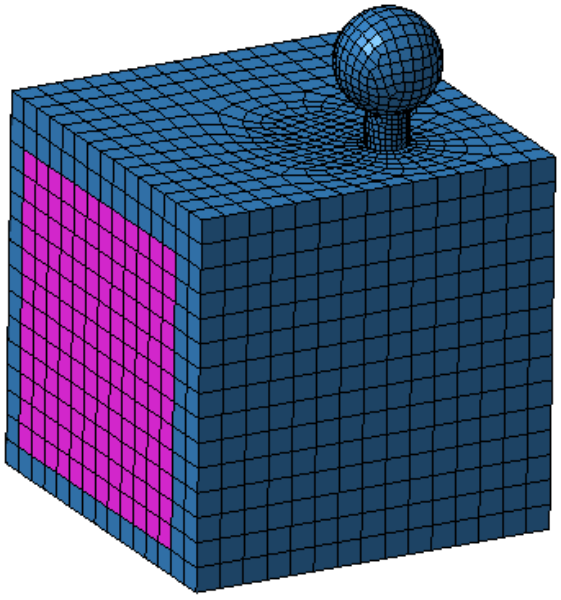

Figure 6.13 BEM model of single room with resonator R1

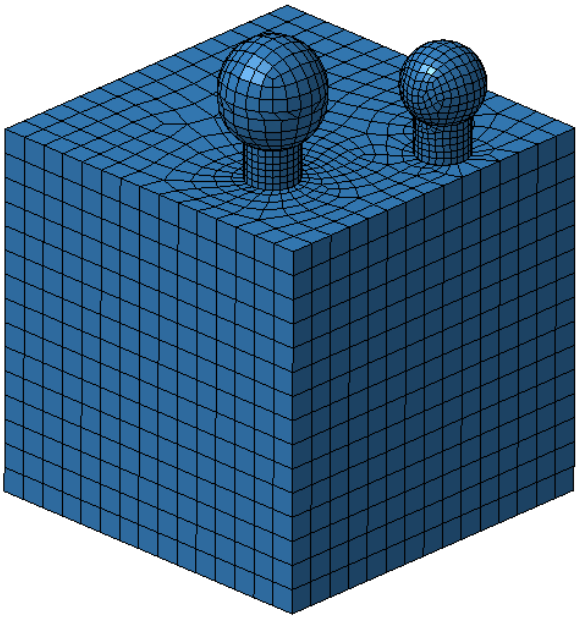

Figure 6.14 BEM model of single room with resonators R1 and R2

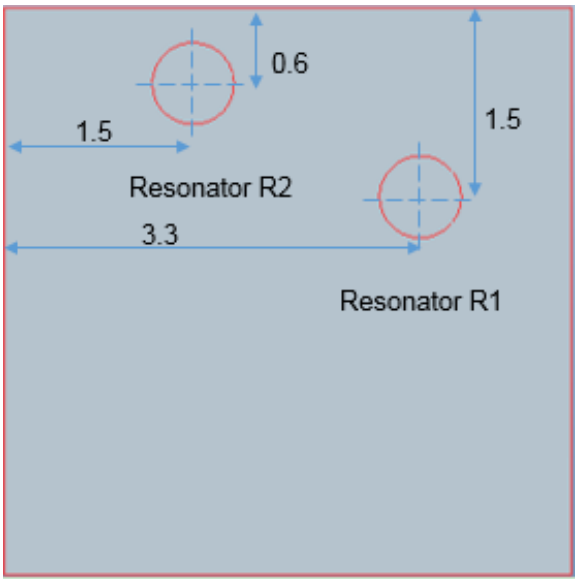

Figure 6.15 Top view of the room indicating the locations of the resonators

Figure 6.16 shows the results for the case with a single resonator which is shown in Figure 6.13. The complete system BEM and FBS prediction compare well up to

200 Hz. This case demonstrates the validity of the approach for lumped impedance modifications. Figure 6.17 shows the same results from 30 to 60 Hz.

Similarly, Figures 6.19 and 6.20 show similar results for the case with two resonators. Notice again the good agreement between the complete system BEM and the FBS prediction up to 200 Hz and especially in the region of the resonance.

The Helmholtz resonators were then replaced with with quarter wave tubes having lengths of 2.28 m and 1.54 m. They were tuned at the same frequencies as the Helmholtz resonators in the prior case. Figure 6.21 compares the sound pressures with the quarter wave tubes to that for Helmholtz resonators. The results indicate that both treatment options are effective.

Thus, FBS can be used to predict the receiver response when lumped impedance modifications are added without BEM remodeling.

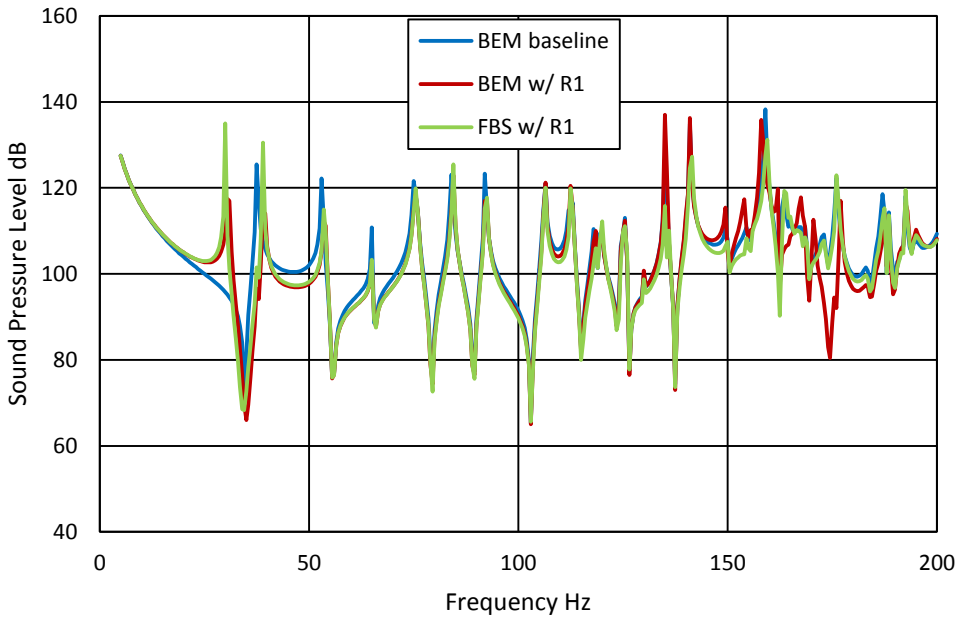

Figure 6.16 Sound pressure at Receiver A with Resonator R1: frequency range of 0~200 Hz

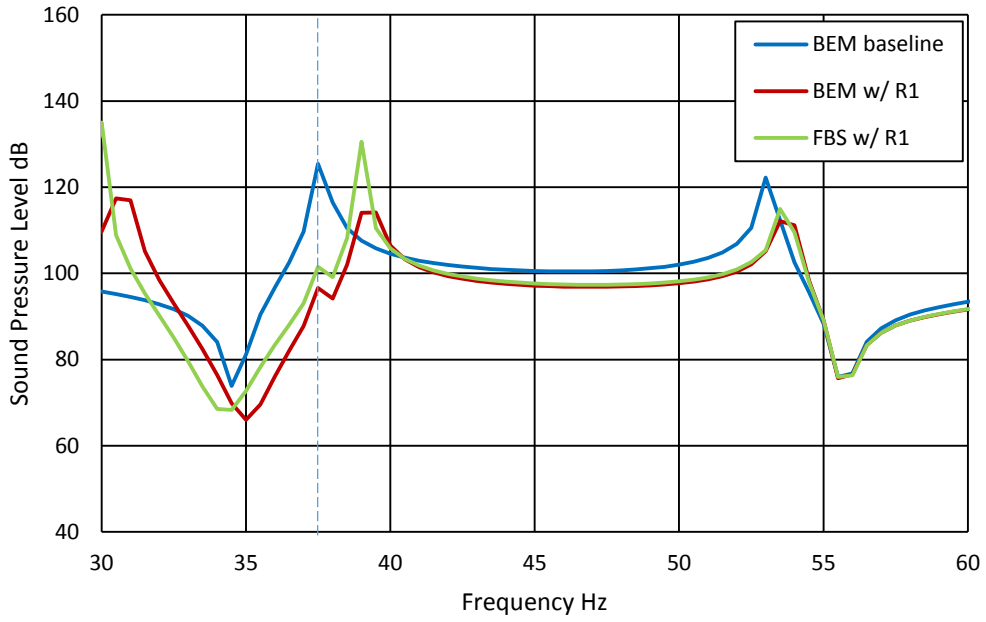

Figure 6.17 Sound pressure at Receiver A with Resonator R1: frequency range of 30~60 Hz

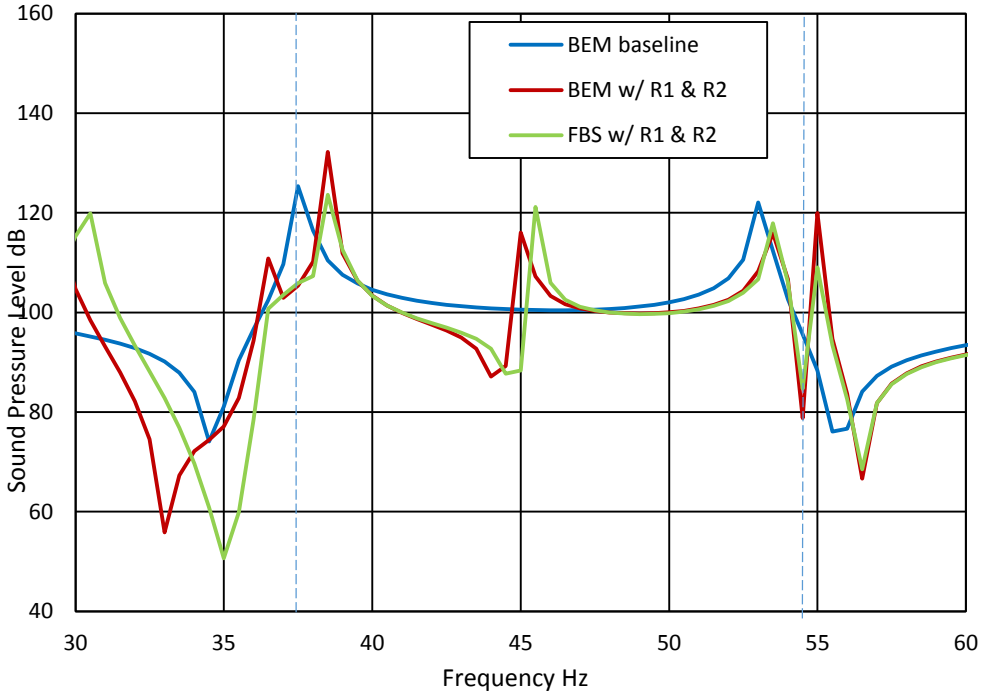

Figure 6.18 Sound pressure at Receiver A with Resonators R1 and R2: turned frequency

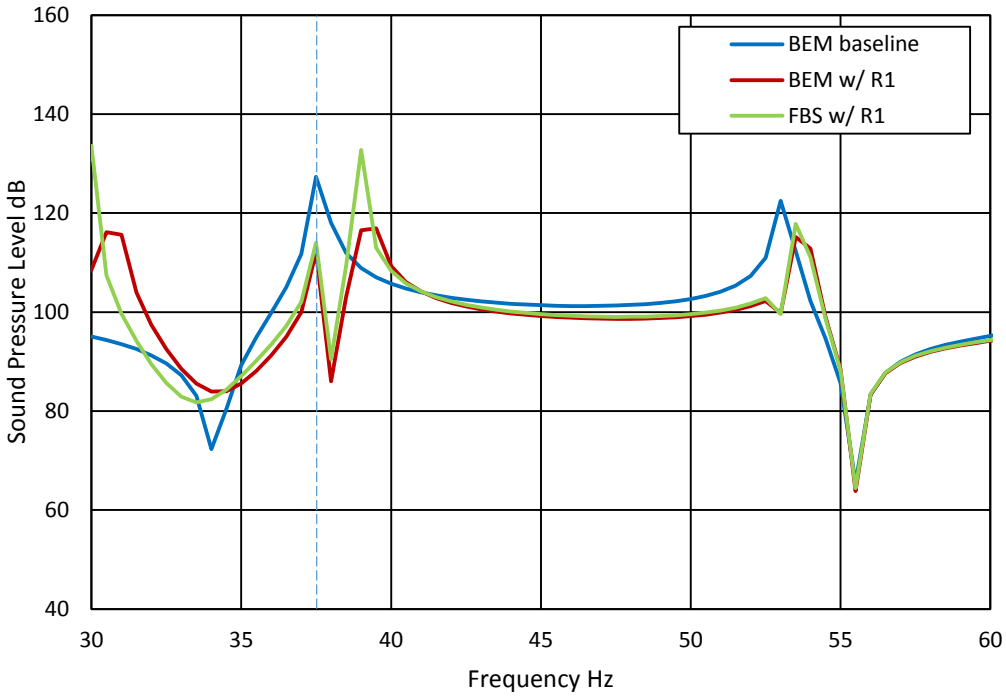

Figure 6.19 Sound pressure at Receiver B with Resonator R1: turned frequency

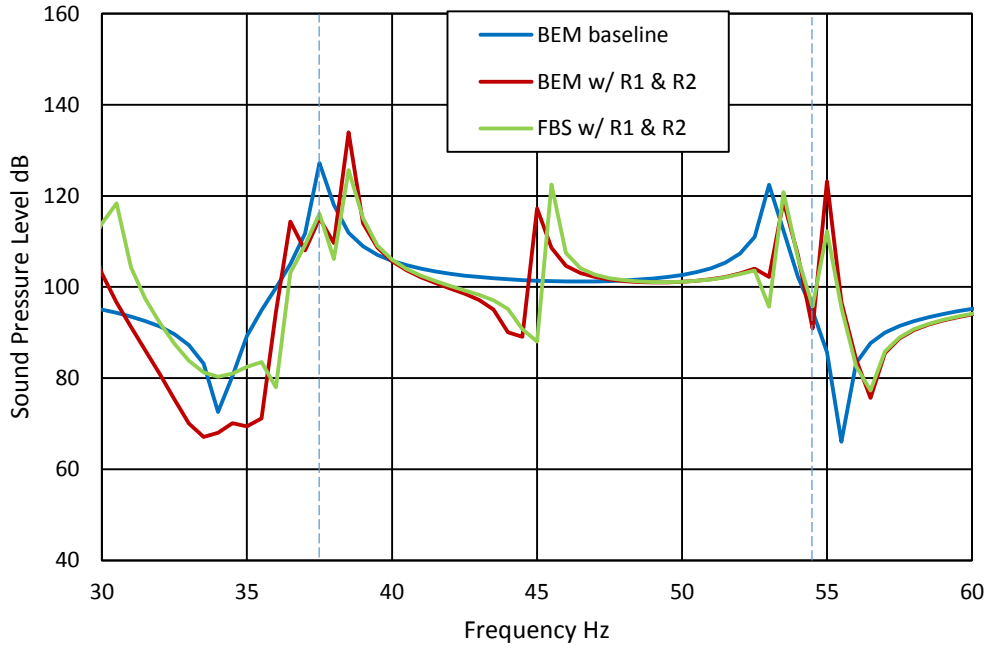

Figure 6.20 Sound pressure at Receiver B with Resonators R1 and R2: turned frequency

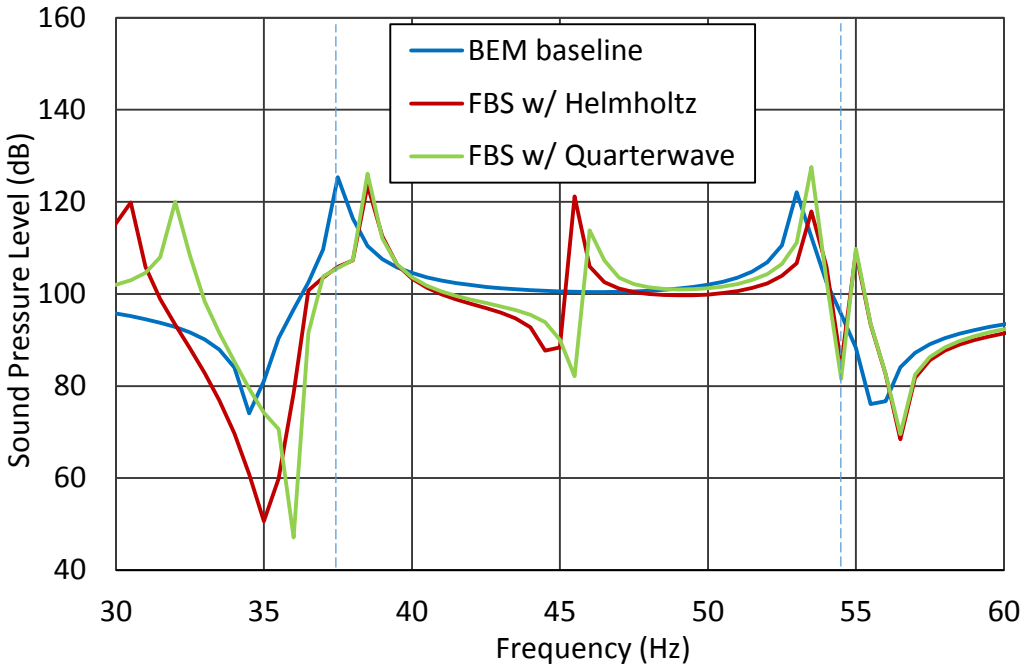

Figure 6.21 Sound pressure at Receiver A with Helmholtz resonators and quarterwave resonators

6.6 Summary

In this chapter, the applications of the FBS method were demonstrated. It was shown that the approach could be used to:

1. Determine the contributions from different airborne connection paths.

2. Determine the effect of adding resonators or glass fiber fill to the connecting ducts.

3. Determine the attenuation due to adding lumped impedance modifications to the subsystems or rooms. Lumped impedance modifications considered included Helmholtz resonators and quarter wave tubes.

In each case, the FBS method proved to be reliable and useful for assessing the impact of modifications without needing to build a new BEM model including the modifications.

Chapter 7

SUMMARY AND FUTURE WORK

7.1 Summary

In this work, frequency based substructuring (FBS), which is commonly used in structural systems, was extended to acoustic systems. Specifically, rooms and connecting ducts between rooms were simulated. FBS provides an approach where subsystems and connections (i.e., rooms and connecting ducts) are simulated and then connected to one another via their respective transfer functions. Transfer functions can be determined using analytical expressions, numerical simulation, or measurement. In so doing, a system model can incorporate components defined by analysis or measurement.

The background of FBS, which is sometimes called transfer path analysis (TPA), was first reviewed. The underlying assumptions were discussed and detailed and the approach was reviewed for structural subsystems. After that, the airborne FBS was derived which serves as the basis for this thesis.

Airborne FBS can be used to determine the contributions from individual sources or connections. Additionally, it can be used to determine the effect of adding attenuation elements to connections or lumped impedances to a component. The method requires that the transfer functions relating the sound pressure to the volume velocity be determined 1) between connection locations, 2) from sources to connection locations, and 2) from sources and connection locations to receivers. These transfer functions can be determined by analysis, experiment, or a

combination of the two. For connections, plane wave propagation is assumed. Accordingly, the sound pressure is assumed to be constant across the cross-section of the duct.

With the theory developed, simulation cases were performed to validate the FBS approach. Boundary element meshes were created using Pro-E and ANSYS, and analyses were performed using LMS Virtual.Lab. A case with two small rooms or enclosures with sources in each room, and two connecting ducts between rooms was considered. Several cases were considered and results from the FBS approach were compared to boundary element simulation of the complete system with good agreement.

The FBS approach was then applied to an enclosure in a hemi-anechoic room with two connecting ducts to the exterior. The approach was demonstrated using measurement. Results obtained using FBS were compared to direct measurement for the entire system. Measured and FBS results were on the same order but there were significant differences. It was suggested that the experiment should be reconsidered and should be the subject of a future research project.

The application of the method was then demonstrated using several examples. It was shown that the FBS approach could be used to determine the contribution to the sound pressure from different connecting ducts. In addition, the effect of adding attenuation elements in the ducts was examined. Finally, lumped impedance modifications were introduced into a room with a source and the effectiveness was determined. Lumped impedance modifications considered included Helmholtz resonators and quarter wave tubes.

The primary weakness of the approach is that plane waves are assumed at the beginning and end of connecting ducts. In addition, it is assumed that the sound pressure is constant across any opening. This limits the applicability of the approach to lower frequencies.

7.2 Future work

There are a number of opportunities for applying this approach in the lab and in industrial applications. It is recommended that the approach first be experimentally applied in a laboratory setting in order to establish the best experimental practices. After which, a more ambitious example can be considered such as a case involving multiple rooms and ducts. In addition, the effectiveness of the approach for suggesting lumped impedance modifications should be considered for a room or enclosure example. The passenger compartment of heavy equipment would appear to be an ideal application.

Appendix A

This section is to determine the volume velocity at the end of the opening of the impedance tube using wave decomposition.

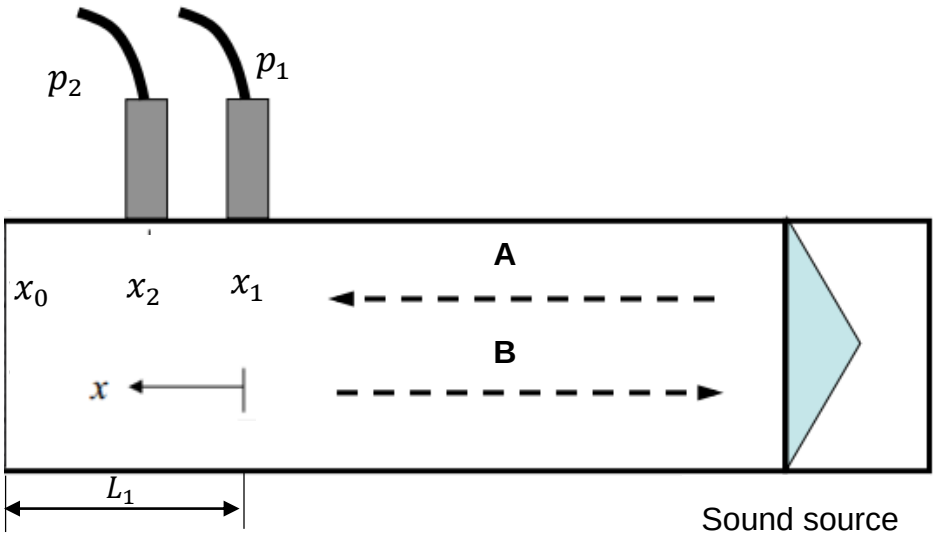

Figure A.0.1 Schematic showing impedance tube setup

Using plane wave decomposition, sound pressure at x_1 and x_2 can be expressed as

$$p_1 = Ae^{-jkX_1} + Be^{jkX_1} \quad \text{(A.1)}$$

and

$$p_2 = Ae^{-jkX_2} + Be^{jkX_2} \quad \text{(A.2)}$$

respectively.

The volume velocity at the tube opening x_0 can be expressed as

$$u_0 = \frac{S_0}{\rho c}(Ae^{-jkX_0} - Be^{jkX_0}) \tag{A.3}$$

Two microphones positioned at x_1 and x_2 measure the sound pressure p_1 and p_2 respectively. The transfer function between the two microphones is determined as

$$H_{12} = \frac{p_2}{p_1} = \frac{Ae^{-jkX_2} + Be^{jkX_2}}{Ae^{-jkX_1} + Be^{jkX_1}} = \frac{e^{-jkX_2} + Re^{jkX_2}}{e^{-jkX_1} + Re^{jkX_1}} \tag{A.4}$$

where

$$R = \frac{B}{A} \tag{A.5}$$

Solve for R:

$$R = \frac{e^{-jkX_2} - H_{12}e^{-jkX_1}}{H_{12}e^{jkX_1} - e^{jkX_2}} \tag{A.6}$$

To make calculations easy, assume $x_1 = 0$, and the phase of p_1 equal zero, which means $\varphi_1 = 0$, thus:

$$p_1 = |p_1| = A + B \tag{A.7}$$

Combining Equations A.5 and A.7, solve for A and B, substitute to Equation A.3:

$$u_0 = \frac{S_0|p_1|}{\rho c(R+1)}(e^{-jkL_1} - Re^{jkL_1}) \tag{A.8}$$

where L_1 is the distance between microphone 1 and the tube opening.

Appendix B

Quarter wave length resonator

A quarter wave length resonator is a simple side branch with closed end. In plane wave region, we assume that the dimensions of the cross-section are much smaller than an acoustic wavelength.

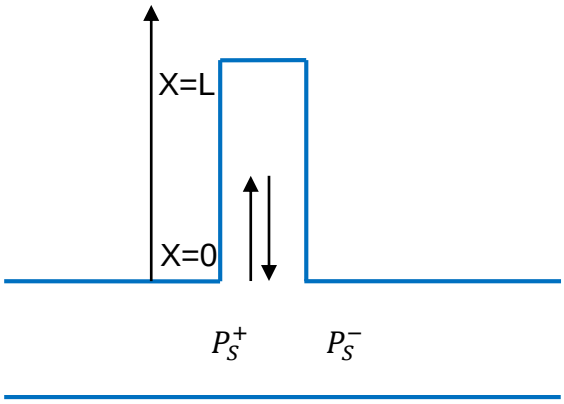

Figure B.1 Quarter wave resonator

The impedance at the opening of the quarter wave resonator can be determined in the following way [26]. The sound pressure and particle velocity can be expressed as:

$$P_S(x) = P_S^+ e^{-jkx} + P_S^- e^{jkx} \tag{B.1}$$

and

$$U_S(x) = (P_S^+ e^{-jkx} - P_S^- e^{jkx})/(\rho_0 c) \tag{B.2}$$

respectively.

Note that x = 0 at the inlet to the branch. In addition, the termination of the branch is rigid so

$$U_S(L) = 0 \tag{B.3}$$

From Equations B.1, B.2, and B.3, the impedance at the inlet of the quarter wave resonator can be expressed as:

$$Z_S = -\frac{j\rho_0 c}{S_B}\cot(kL_B) \tag{B.4}$$

The resonator will be most effective if the impedance at the opening is 0 and is analogous to a short circuit in an electrical system. That will be the case when:

$$kL_B = \frac{n\pi}{2}, n = 1,3,5, \ldots \tag{B.5}$$

It follows that the length of side branch will be:

$$L_B = \frac{nc}{4f} = n(\frac{\lambda}{4}), n = 1,3,5, \ldots \tag{B.6}$$

where n is an integer. This resonator type is often referred to as a quarter wave tube because it is effective at multiples of a quarter wave length.

Helmholtz resonator

A Helmholtz resonator is a side branch with a narrow neck and a large volume body. In plane wave region, the dimensions of the cross-section are much smaller than an acoustic wavelength.

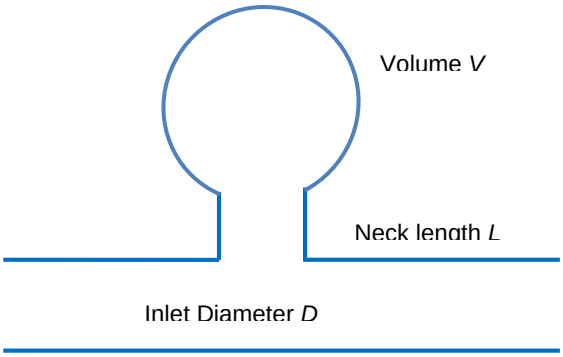

Figure B.2 Helmhotz resonator

The impedance at the opening of the Helmholtz resonator can be determined in the following way [26]. The inlet impedance in terms of sound pressure and volume velocity can be expressed as:

$$Z_S = \frac{P_S}{v_S S_B} = \frac{jk\rho_0 cL}{S_B} + \frac{\rho_0 c}{jkV_0} \tag{B.7}$$

Note that x = 0 at the inlet to the branch. In addition, the termination of the branch is rigid so

$$v_S(L) = 0 \tag{B.8}$$

From Equations B.7, B.8, and B.9, the impedance at the inlet of the quarter wave resonator can be expressed as:

$$Z_S = \frac{P_S}{v_S S_B} = -\frac{j\rho_0 c}{S_B}\cot(kL_B) \tag{B.9}$$

The resonator will be most effective if the impedance at the opening is 0 and is analogous to a short circuit in an electrical system. That will be the case when:

$$f = \frac{c}{2\pi}\sqrt{\frac{S_B}{LV_0}} \tag{B.10}$$

which is also called the eigenfrequency of the Helmholtz resonator.

Due to the different connection condition between the Helmholtz resonator volume and the enclosure system, there will be an incompressible near field around the opening, which will increase the effective length of the resonator neck by ΔL. This end corrections are proportional to the cross sectional dimension of the neck. For a circular cross section neck, the increased amount of length can be expressed as:

$$\Delta L = 0.82\ D/2 \text{ (baffled inlet)} \tag{B.11a}$$

$$\Delta L = 0.61 D/2 \text{ (inlet in a free field)} \tag{B.11b}$$

The Equation (B.11a) expresses the situation when the resonator is connect to a large wall compared to the sound wave length. The Equation (B.11b) is applied when the resonator is connected far away from any reflecting surfaces.

References

[1] Jetmundsen, B., R. L. Bielawa, and W. G. Flannelly. "Generalized frequency domain substructure synthesis." *Journal of the American Helicopter Society* 33.1 (1988): 55-64.

[2] Gordis, J. H., R. L. Bielawa, and W. G. Flannelly. "A general theory for frequency domain structural synthesis." *Journal of Sound and Vibration* 150.1 (1991): 139-158.

[3] Avitabile, P. "Twenty years of structural dynamic modification-a review." *Journal of Sound and Vibration* 37.1 (2003): 14-27.

[4] De Klerk, D., D. J. Rixen, and S. N. Voormeeren. "General framework for dynamic substructuring: history, review and classification of techniques." *AIAA journal* 46.5 (2008): 1169-1181.

[5] Craig Jr., R. R. "A review of time-domain and frequency-domain component mode synthesis method." *International journal of Analytical & Experimental Modal Analysis* 2, 2 (1987), 59–72.

[6] Kailath, T. Linear Systems. Prentice-Hall, 1980. ISBN: 0-135-36961-4.

[7] Imregun, M., and D. J. Ewins. "Realisation of complex mode shapes." *Proceedings of the 11th Annual International Modal Analysis Conference*. 1993.

[8] Bolt, R.H. and K.U. Ingard. “System Considerations in Noise Control Problems. Handbook of Noise Control”, First Edition, edited by C.M. Harris. New York: McGraw-Hill. 1957.

[9] Verheij, J. W. "Multi-path sound transfer from resiliently mounted shipboard machinery: Experimental methods for analyzing and improving noise control." PhD thesis, 1982.

[10] Magrans, F. X. "Method of measuring transmission paths." *Sound and Vibration* 74.3 (1981): 321-330.

[11] Sottek, R. "An artificial head which speaks from its ears: investigations on reciprocal transfer path analysis in vehicles, using a binaural sound source." *SAE noise and vibration conference and exhibition*, Traverse City, Michigan, USA. 2003.

[12] Plunt, J. "Finding and fixing vehicle NVH problems with transfer path analysis." *Sound and Vibration* 39.11 (2005): 12-17.

[13] Van der Auweraer, H. “Transfer path analysis in the critical path of vehicle refinement: the role of fast, hybrid and operational path analysis.” *SAE Technical Paper* (2007), No. 2007-01-2352.

[14] Van der Linden, P. J. G., "Body in white panel noise assessment through spatial and modal contribution analysis." *Proceedings of the international seminar on modal analysis.* Vol. 3. KU Leuven; 1998, 2001.

[15] Plunt, J. "Examples of using transfer path analysis (TPA) together with CAE-models to diagnose and find solutions for NVH problems late in the vehicle development process." *SAE paper* (2005): 01-2508.

[16] Liu, D. "Applying Transfer Path Analysis to Automotive Interior Noise and Vibration Refinement and Development [J]." *Noise and Vibration Control* 4 (2007): 023.

[17] Hashioka, M., and I. Kido. "An application technique of transfer path analysis for automotive body vibration." *SAE paper* (2007): 01-2334.

[18] Karlsson, S.E.S. “Identification of external structure loads from measured harmonic responses”, *Journal of Sound and Vibration*, 196 (1) (1996), pp. 59–74

[19] Janssens, K. "OPAX: A new transfer path analysis method based on parametric load models." *Mechanical Systems and Signal Processing* 25.4 (2011): 1321-1338.

[20] Gajdatsy, P. "Application of the transmissibility concept in transfer path analysis." *Mechanical Systems and Signal Processing* 24.7 (2010): 1963-1976.

[21] Yang, K. T., and Y. Park. "Joint structural parameter identification using a subset of frequency response function measurements." *Mechanical Systems and Signal Processing* 7.6 (1993): 509-530.

[22] Lee, D., and W. Hwang. "An identification method for joint structural parameters using an FRF-based substructuring method and an optimization technique." *Journal of mechanical science and technology* 21.12 (2007): 2011-2022.

[23] Zheng, J., F. J. Fahy, and D. Anderton. "Application of a vibro-acoustic reciprocity technique to the prediction of sound radiated by a motored IC engine." *Applied Acoustics* 42.4 (1994): 333-346.

[24] Fahy, F. J. "The vibro-acoustic reciprocity principle and applications to noise control." Acta Acustica united with Acustica 81.6 (1995): 544-558.

[25] Zhou, L., D. Herrin, and T. Wu, "Simulation of enclosures including attached duct work," *SAE Int. J.Passeng. Cars - Mech. Syst.* 6(2):2013, doi:10.4271/2013-01-1958.

[26] Wallin, H. P. “Sound and vibration”. Institutionen för farkostteknik, Tekniska högskolan, 2010.

[27] Seybert, A. F., and T. W. Wu. “Acoustic Modeling: Boundary Element Methods,” Encyclopedia of Acoustics, Chapter 15, Malcolm J. Crocker, ed., John Wiley and Sons, Inc., New York, pp. 173-184, 1997.

[28] Munjal, M. L. Acoustics of ducts and mufflers. John Wiley & Sons, 2014.

[29] Mechel, F. P., ed. Formulas of acoustics. Vol. 2. Springer, 2002.

[30] ASTM C522 - 03(2009), Standard Test Method for Airflow Resistance of Acoustical Materials, http://www.astm.org/Standards/C522.htm

[31] Genuit, K. "The sound quality of vehicle interior noise: a challenge for the NVH-engineers." *International journal of vehicle noise and vibration* 1.1 (2004): 158-168.

[32] De Sitter, G, "Operational transfer path analysis." *Mechanical Systems and Signal Processing* 24.2 (2010): 416-431.

[33] Lohrmann, M. and T. Hohenberger. "Operational transfer path analysis: comparison with conventional methods." *Journal of the Acoustical Society of America* 123.5 (2008): 3534.

[34] De Klerk, D., and A. Ossipov. "Operational transfer path analysis: Theory, guidelines and tire noise application." *Mechanical Systems and Signal Processing* 24.7 (2010): 1950-1962.

[35] Jetmundsen, B. “On Frequency Domain Methodologies for Structural Modification and Sub-system Synthesis”. PhD thesis, Rensselaer Polytechnic Institute, Troy, NY, 1986.

[36] Gordis, J. H. "Structural synthesis in the frequency domain: a general formulation." *Shock and Vibration* 1.5 (1994): 461-471.

[37] D'Ambrogio, W., and A. Sestieri. "A unified approach to substructuring and structural modification problems." *Shock and Vibration* 11.3 (2004): 295-309.

[38] Nicgorski, D., and P. Avitabile. "Experimental issues related to frequency response function measurements for frequency-based substructuring." *Mechanical Systems and Signal Processing* 24.5 (2010): 1324-1337.

[39] Allen, M. S., and R. L. Mayes. "Comparison of FRF and modal methods for combining experimental and analytical substructures." *Proceedings of the 25th International Modal Analysis Conference*, Orlando, FL. 2007.

[40] Carne, T. G., and C. R. Dohrmann. "Improving experimental frequency response function matrices for admittance modeling." *Proceedings of the Nineteenth International Modal Analysis Conference*. 2006.

[41] Crowley, J. R., "Direct structural modification using frequency response functions." *Proceedings of the second international modal analysis conference*. 1984. pp. 58–65

[42] Klosterman, A. L. “On the experimental determination and use of modal representations of dynamic characteristics”. PhD thesis, University of Cincinnati, 1971.

[43] Liu, W. “Structural dynamic analysis and testing of coupled structures”. PhD thesis, University of London, 2001.

[44] Mayes, R. L., and E. C. Stasiunas. "Combining lightly damped experimental substructures with analytical substructures." *Proceedings of the Twentyfifth International Modal Analysis Conference*, Orlando, FL. 2007.

[45] Kim, S. H. "A study on the hybrid frf based substructuring (FBS) application to vehicle subframe." *International Conference on Sound and Vibration*, ICSV12. 2005.

[46] Lim, T. C., and J. Li. "A theoretical and computational study of the FRF-based substructuring technique applying enhanced least square and TSVD approaches." *Journal of Sound and Vibration* 231.4 (2000): 1135-1157.

[47] Sjövall, P. “Identification and Synthesis of Components for Vibration Transfer Path Analysis”. PhD thesis, Chalmers University of Technology, 2007.

[48] Rixen, D. "How measurement inaccuracies induce spurious peaks in frequency based substructuring." *Proceedings of the Twenty Sixth International Modal Analysis Conference*, Orlando, FL. 2008.

[49] Rixen, D. J. T., E. P. Godeby, and E. Pagnacco. "Dual assembly of substructures and the fbs method: Application to the dynamic testing of a guitar." *Proceedings of the Twenty Eighth International Conference on Noise & Vibration Engineering (ISMA)*. 2006.

[50] Snowdon, J. C. “Mechanical four-pole parameters and their application”, *Journal of Sound and Vibration* 15(3), 307-323, 1971.

[51] Lee, D. H., W. S. Hwang, and C. M. Kim, “Design sensitivity analysis and optimization of an engine mount system using an FRF-based Substructuring method,” *Journal of Sound and Vibration* 255(2), 383-397, 2002.

[52] De Klerk, D. and D. J. Rixena, “Component transfer path analysis method with compensation for test bench dynamics,” *Mechanical Systems and Signal Processing*, 24, 1963-1710, 2010.

[53] Norwood, C. J. and J. D. Dickens, “The effect of vibration isolator properties and structural stiffness on isolator performance,” *Journal of Vibration Control*, 4:253, 1998.

[54] Munjal, M. L. “Acoustics of Ducts and Mufflers”, Wiley, New York, 1987.

[55] Lim, T. C. and G. C. Steyer, “System dynamics simulation based on structural modification analysis using response techniques,” *Proc.10th International Modal Analysis Conference*, 1, 1153-1158, 1992.

[56] Otte, D., J. Leuridan, H. Grangier and R. Aquilina, "Prediction of the dynamics of structural assemblies using measured FRF-data: some improved data enhancement techniques," *Proc. of 9th International Modal Analysis Conference*, 909-918, 1991.

[57] Verheij, J. W. “Multi-path sound transfer from resiliently mounted shipboard machinery: Experimental methods for analyzing and improving noise control,” Ph.D. Dissertation, 1982.

[58] Wyckaert, K. and H. Van der Auweraer, “Operational analysis, transfer path analysis, modal analysis: Tools to understand road noise problems in cars,” *Ingénieurs de l'automobile*, 698, 30-33, 1995.

[59] LMS, “Transfer Path Analysis-The qualification and quantification of vibro-acoustic transfer paths,” see http://www.lmsintl.com/downloads/cases.

[60] Verheij, J. W. "Experimental procedures for quantifying sound paths to the interior of road vehicles." *Proc. of 2nd international conference on vehicle comfort*, part, 1, 483-491, 1992.

[61] Van Der Linden, P. J. G. and J. K. Fun, "Using mechanical-acoustical reciprocity for diagnosis of structure borne sound in vehicles," *Le Journal de Physique* 4, C5-93, 1994.

[62] De Vis, D. and W. Hendricx, "Development and integration of an advanced unified approach to structure borne noise analysis." *Proc. of INTER-NOISE and NOISE-CON Congress and Conference*, 2, 561-564, 1992.

[63] De Geest, E. and H. Patzold, "Comparison between room transmission functions calculated with a boundary element method and a ray tracing method including phase," *Proc. of International congress on noise control engineering*, 3177-3180, 1996.

[64] Hodgson, M. “On the prediction of sound fields in large empty rooms,” *Journal of the Acoustical Society of America*, 84, 253, 1988.

[65] Liu, J., "Advanced studies on series impedance in waveguides with an emphasis on source and transfer impedance" PhD dissertation. 2011.

[66] Wolff, O. and R. Sottek. "Panel Contribution Analysis - An Alternative Window Method," *SAE Technical Paper* 2005-01-2274, 2005, doi:10.4271/2005-01-2274.

[67] COMESAÑA, D. F. "Comparison of inverse methods and particle velocity based techniques for transfer path analysis." *Acoustics 2012 Nantes* (2012).

[68] Koners, G., "Panel Noise Contribution Analysis: An Experimental Method for Determining the Noise Contributions of Panels to an Interior Noise," *SAE Technical Paper* 2003-01-1410, 2003, doi:10.4271/2003-01-1410.

[69] Cariou, C. "Tool for interior noise sources detection in aircraft with comparison of configurations." Berlin Beamforming Conference. 2012.

[70] He, R., L. Zhou, and D. Herrin, “Simulation of airborne paths using frequency based substructuring”, Inter.Noise 2015, San Francisco, USA 2015

[71] He, R., and D. Herrin, “Applications of airborne path frequency based substructuring,” Inter.Noise 2015, San Francisco, USA 2015

[72] Levine, H., and J. Schwinger, "On the radiation of sound from an unflanged circular pipe." Physical review 73.4 (1948): 383.

[73] Pierce, AD., and RT. Beyer, "Acoustics: an introduction to its physical principles and applications." The Journal of the Acoustical Society of America 87.4 (1990): 1826-1827.

VITA

Rui He was born in Anhui, China. He received the Bachelor's degree of Engineering in Automotive Engineering from Harbin Institute of Technology, China in July 2011 with honors. He joined in graduate school at the University of Kentucky for Master's degree in Mechanical Engineering in January 2012. He has been assigned teaching assistant for undergraduate courses for one and half years. During graduate study, he had two conference papers published on Inter.Noise 2015, and was awarded Young Professionals Grant. He had an internship as a Mechanical Engineer at Western Digital from June to August 2013. He joined HGST, a Western Digital company, as a full time Senior Mechanical/Dynamics Engineer since December 2013.

Rui He